Geochimica et Cosmochimica Acta
September 2016, Volume 189, Pages 214-235
http://dx.doi.org/10.1016/j.gca.2016.06.005
http://archimer.ifremer.fr/doc/00341/45255/

Comparative geochemistry of four ferromanganese crusts from the Pacific Ocean and significance for the use of Ni isotopes as paleoceanographic tracers

Gueguen Bleuenn [1, 2, *], Rouxel Olivier [2], Rouget Marie-Laure [3], Bollinger Claire [3], Ponzevera Emmanuel [2], Germain Yoan [2], Fouquet Yves [2]

[1] Institut Universitaire Européen de la Mer, UMR 6538, Université de Bretagne Occidentale, 29280 Plouzané, France
[2] IFREMER, Centre de Brest, Unité Géosciences Marines, 29280 Plouzané, France
[3] Institut Universitaire Européen de la Mer, UMS 3113, Université de Bretagne Occidentale, 29280 Plouzané, France

* Corresponding author : Bleuenn Gueguen, email address : bleuenn.gueguen@univ-brest.fr

Abstract :

Ferromanganese (Fe-Mn) crusts are potential archive of the Ni isotope composition of seawater through time. In this study we aim at (1) understanding Ni isotope fractionation mechanisms and metal enrichment processes in Fe-Mn deposits, (2) addressing global vs. local control of Ni isotope composition of these deposits. Two Fe-Mn crusts from the North Pacific Ocean (Apuupuu Seamount, Hawaii) and two Fe-Mn crusts from the South Pacific Ocean (near Rurutu Island, Austral archipelago of French Polynesia) were characterized for their elemental geochemistry and Ni isotope composition. Geochemical analyses were performed at millimeter intervals in order to provide time-resolved record of Ni isotopes. Chronology and growth rates were determined using cosmogenic 10Be isotope abundances. The results show that, despite different growth rates, textures and geochemical patterns, Fe-Mn crusts from both North and South Pacific Oceans have fairly homogenous Ni isotope compositions over the last ~17 Ma, yielding average δ60/58Ni values of 1.79 ±0.21 ‰ (2sd, n=31) and 1.73 ±0.21 ‰ (2sd, n=21) respectively. In one crust sample, however, layers directly in contact with the altered substrate show anomalously light δ60/58Ni values down to 0.25 ±0.05 ‰ (2se) together with rejuvenated 10Be/9Be ratios correlating with elevated Ni/Mn ratios. Such patterns are best explained by protracted fluid–rock interactions leading to alteration of Mn-phases after crust formation. Isotopically light Ni is best explained by Ni isotope fractionation during adsorption rather than the contribution of external Ni sources (e.g. hydrothermal sources) having light Ni isotope compositions. The combination of our results with previously published data on Fe-Mn crusts indicates that the average Ni isotope composition in deep waters has not changed through the Cenozoic (~70 Ma). We propose that Ni isotope variations in Fe-Mn crusts may not only record variations of Ni sources to the oceans, but also post-depositional processes depending on the growth history and geological settings of Fe-Mn crusts.

Keywords : Ferromanganese crusts ; Nickel isotopes ; Paleoceanography ; Pacific Ocean; Biogeochemical cycling

1. Introduction

Fe-Mn crusts are seafloor metalliferous deposits forming through slow accumulation of seawater-derived Fe- and Mn-oxyhydroxide colloids on hard substrates such as volcanic seamounts that are kept sediment-free for millions of years (Craig et al., 1982; Halbach et al., 1983; Hein et al., 1988; Hein et al., 1992; Koschinsky and Halbach, 1995). Fe-Mn crusts are particularly abundant in the Northwest Pacific, e.g., the Pacific Prime Zone (Hein et al. (2013) and in the South Central Pacific (e.g., French Polynesia; Kosakevitch, 1987; Pichocki and Hoffert, 1987; Lesuave et al., 1989; Kosakevitch and Disnar, 1997) in connection with the formation and aging of Jurassic to Cretaceous volcanic seamounts (Halbach et al., 1983; Halbach and Puteanus, 1984; Halbach et al., 1984; Aplin and Cronan, 1985; De Carlo et al., 1987; Hein et al., 1988; Hein et al., 1992). A seawater origin for trace metals incorporated into Fe-Mn crusts has been well documented using isotopic and trace element geochemical signatures including rare earth elements (Bonatti and Joensuu, 1966; Bonatti et al., 1972; De Carlo et al., 1987; Nicholson et al., 1997; Hein et al., 2012; Bau et al., 2014). The importance of oceanographic parameters such as the depth of the oxygen-minimum-zone (OMZ), the calcite-compensation-depth (CCD) and phosphatization events that occurred during the Cenozoic have been well-recognized to influence Fe-Mn crusts geochemical composition (Hein et al., 1993). Hydrothermal input of metals have been also suggested in some cases (van de Flierdt et al., 2004; Chu et al., 2006; Horner et al., 2015) which is in line with the recognition that hydrothermal venting may impact regionally the inventory of metals, in particular Fe, in the deep ocean (Toner et al., 2009; Tagliabue et al., 2010; Conway and John, 2014; Fitzsimmons et al., 2014). In rare cases, cosmic spherules were also reported in South Pacific crusts (Kosakevitch, 1987; Halbach et al., 1989; Lesuave et al., 1989; Kosakevitch and

Disnar, 1997) but it remains unclear whether such extra-terrestrial input could affect bulk Fe-Mn crusts composition.

Radiogenic isotope geochemistry (Pb, Sr, Nd, Os, Hf) in Fe-Mn crusts has been extensively investigated in order to resolve fundamental paleoceanographic processes such as the evolution of oceanic circulation resulting from opening or closure of oceanic passages (e.g. closure of the Panama gateway, opening of the Drake passage), modifications in continental erosion fluxes after major climatic changes (von Blanckenburg et al., 1996b; Abouchami et al., 1997; Ling et al., 1997; O'Nions et al., 1998; Frank et al., 1999; Reynolds et al., 1999; Frank, 2002; Frank et al., 2002; van de Flierdt et al., 2003; Ling et al., 2005; Peate et al., 2009; Chen et al., 2013), and the impact of hydrothermal inputs (van de Flierdt et al., 2004). It should be noted that most of these studies were carried out on samples from the North Central Pacific Ocean. However other oceanic regions, including the South Pacific, have also important Fe-Mn crusts deposits (Hein et al., 2013) and they are poorly documented.

Stable isotope composition of metals (e.g., Fe, Zn, Ni, Cd, Cu, Tl, Mo) in Fe-Mn crusts and nodules, provide interesting proxies to unravel changes in the marine sources and biogeochemical cycles of metals through time (Zhu et al., 2000; Barling et al., 2001; Rehkämper et al., 2002; Siebert et al., 2003; Levasseur et al., 2004; Rehkämper et al., 2004; Anbar and Rouxel, 2007; Schmitt et al., 2009; Horner et al., 2010; Nielsen et al., 2011; Horner et al., 2015). However, the application of Ni stable isotopes as paleoceanographic proxies is not straightforward since at least three processes may affect the Ni isotope records preserved in Fe-Mn crusts: (1) changes in the relative fluxes of Ni sources and sinks in the ocean, (2) internal biogeochemical cycling of Ni and water mass mixing, and (3) fractionation processes during Ni incorporation at the Fe-Mn crust surface (Wasylenki et al., 2008; Wasylenki et al., 2011; Gueguen, 2013; Nielsen et al., 2013; Wasylenki et al., 2014a;

Wasylenki et al., 2014b; Bryan et al., 2015) and Ni distribution among Mn-phases (Koschinsky and Halbach, 1995; Koschinsky and Hein, 2003).

The isotope composition of Ni in marine systems has recently attracted significant attention (Cameron and Vance, 2014) owing to its nutrient-type behavior (Sclater et al., 1976; Cameron and Vance, 2014), and multiple sources in seawater (e.g., rivers, atmospheric depositions, hydrothermal vents; Gall et al., 2013; Cameron and Vance, 2014; Little et al., 2015). In a reconnaissance study, Gall et al. (2013) reported up to 1.6 ‰ variations in $\delta^{60/58}$Ni ($\delta^{60/58}Ni = (^{60}Ni/^{58}Ni_{sample}/^{60}Ni/^{58}Ni_{NIST986} - 1) \times 1000$; see section 2.3) along the growth layers of Fe-Mn crusts from various ocean basins. The apparent absence of relationship between Ni isotope variability and sample locations and depths implies that differences in water masses, surface water productivity and bottom water oxygenation have no influence on Ni isotope signatures preserved in Fe-Mn crusts. The Ni isotope composition of surface scrapings of Fe-Mn crusts also shows significant variations in $\delta^{60/58}$Ni (from 0.9 to 2.5 ‰) with values being both heavier and lighter than the modern seawater value determined at 1.44 ±0.15‰ (Cameron and Vance, 2014). While it has been argued that heavier Ni isotopes values may be due to continental input and lighter Ni isotope values reflecting the extent of hydrothermal input in deep waters (Gall et al., 2013), it remains unclear which processes are controlling Ni isotope record in Fe-Mn crusts. Presumably, the importance of local or post-depositional effects associated with Ni adsorption and precipitation in Fe-Mn crusts should also be considered as a potential cause of isotope fractionation as suggested by experimental results of Ni sorption on Fe-oxyhydroxides (Sorensen et al., 2011; Gueguen, 2013; Wasylenki et al., 2015) and Mn-oxyhydroxides (Gueguen, 2013; Wasylenki et al., 2014a) indicating enrichment of the mineral phase in light Ni isotopes, keeping in mind that Ni is essentially hosted in the Mn-phase.

Here, we report Ni isotope composition of two pairs of Fe-Mn crusts collected on two volcanic seamounts from the Northern Pacific Ocean (Apuupuu Seamount, Hawaii) and the Southern Pacific Ocean (near Rurutu Island, Austral archipelago of French Polynesia). This approach allows (a) a direct comparison of Ni isotope record in Fe-Mn crusts from the same seamount in order to address local effects, and (b) a comparison of geochemical composition of crusts between North and South Pacific in order to address the effect of more global geochemical processes. Through a high-resolution profile of major and trace element compositions, ^{10}Be dating and Ni isotope ratios, we tested the following hypotheses: (1) secular variations of Ni isotope in deep seawater should be reflected by co-variations in crusts recovered from the same locality, while differences should provide clues for post-depositional or local effects (2) differences between North and South Pacific crusts should provide information regarding the importance of oceanographic parameters (e.g., water masses) and the potential influence of hydrothermal sources.

2. Materials and methods

2.1. Sample description and microsampling

Two Fe-Mn crusts (samples J2-480 and J2-480-R14) were collected by the Remotely Operated Vehicle (ROV) Jason2 (Woods Hole Oceanographic Institution) on Apuupuu Seamount (155°25'W, 18°32'N), about 50 km south of Mauna Loa Volcano in Hawaii, at ~2000 m water depth during the FeMO cruise (R/V Kilo Moana, University of Hawaii) in October 2009 (Figure 1). Although the samples from Apuupuu Seamount were sampled by using a ROV allowing a precise determination of sample location and depth, sample J2-480 could not be located since it originated from a set of samples that got mixed together in the

ROV sampling basket. In addition, sample J2-480 was not collected attached to its substrate in contrast to sample J2-480-R14. The total thickness of both Apuupuu crusts was ~60 mm. These samples will be referred in the paper as “North Pacific Fe-Mn crusts”.

Two other Fe-Mn crusts (samples ZEP2-DR-05-04 and ZEP2-DR-06-03) were collected by dredging in the South Pacific in the proximity of the Rurutu Island (22°S, 150°W), Austral archipelago of French Polynesia, at 1826 m and 1530 m water depth during the ZEPOLYF2 cruise (R/V L’Atalante, Ifremer-Genavir) in July-August 1999. During this cruise, 24 dredges recovered volcanoclastic sediments, altered and fresh pillow basalts, hyaloclastites and Fe-Mn crusts (Bonneville et al., 2006; Adam and Bonneville, 2008) along the Cook-Austral volcanic chains in South Pacific. These samples will be referenced in this paper as “South Pacific Fe-Mn crusts”. Sample ZEP2-DR05-04 consisted of 25 mm thick Fe-Mn crusts attached to a brecciated basalt substrate mixed with minor phosphorites and carbonates. Sample ZEP2-DR06-03 consisted of 90 mm thick Fe-Mn crusts lacking evidences for substrate attached at its bottom. In all cases, the smooth aspect of the top surface has been used to determine growth direction. Fe-Mn crust samples were further divided into two parts: the “top” corresponding to the surface of the crust in contact with seawater, the “middle” when no substrate was collected attached to the crust or the “bottom” when contact with the substrate is recovered. Based on mineral textures (see section 3) ZEP2-DR05-04 crust was further divided into subsections inner region “I" and outer region "O" (Figure 2).

The outermost layer of each crust (20 to 25 mm in thickness) was cut and embedded in epoxy resin. The surface was polished for petrographic examination and spatially resolved geochemical analyses (see below). Fe-Mn crusts were then subsampled with a microdrilling device (New Wave Micromill®). Layers perpendicular to the direction of growth were drilled to obtain a high-resolution microsampling every 1 to 2 mm of the crust growth layers (Figure

2). Powders from the same layer were mixed and stored in small plastic centrifuge tubes to obtain a total amount of powder between ~30 and 50 mg.

2.2. Major and trace elements concentrations measurement

Between 10 and 20 mg of powdered samples were weighed in Teflon vials and digested in a mixture of 5 mL concentrated HNO_3 and 5 mL 6 mol/L HCl. After evaporation at 80°C on hot plates, the solid residue was dissolved with 5 mL of 6 mol/L HCl and then evaporated to dryness at 80°C. This operation was reiterated once to ensure efficient dissolution of the samples. Solid residues were dissolved in 10 mL 6 mol/L HCl and kept as archive solutions. Reagents used for digestion and chemical procedures were prepared from sub-boiled distilled concentrated hydrochloric and nitric acids using a Cleanacids® device (Analab, France).

Major and trace elements concentrations were measured by Quadrupole Inductively Coupled Plasma Mass Spectrometry (ICP-MS) (X-Series 2, Thermo-Finnigan) at the Pôle-Spectrométrie-Océan (IUEM-Ifremer, Brest, France) (Table 1) and precision was generally better than 5%. Geological reference materials of manganese nodules Nod-A-1 and Nod-P-1 (US Geological Survey) were systematically analyzed along with samples and the measured concentrations fell within 10% uncertainty of the published concentration values (not shown).

2.3. Nickel isotope analysis

Nickel isotopes were measured at the Pôle-Spectrométrie-Océan (IUEM-Ifremer, Brest, France) by MC-ICP-MS (Neptune, Thermo Scientific). Nickel was separated from the geological matrix by ion-exchange chromatography columns involving two steps. First, the

dissolved samples were processed through AG1-X8 resin in 6 mol/L HCl to separate Ni from Fe, Zn and most of Co and Cu that are retained on the column. Elution of Ni was made in 6 mol/L HCl. Afterwards, Ni was purified with Ni-spec resin (Eichrom) by complexation of Ni with a DMG (Dimethylglyoxime) molecule allowing elution of the remaining matrix elements. Eluted Ni fractions were evaporated and dissolved in 0.28 mol/L HNO_3 for MC-ICP-MS analyses. The experimental and analytical method is described in details in Gueguen et al. (2013). Nickel isotope ratios were corrected from instrumental mass bias using the double-spike method as described in Gueguen et al. (2013). The double-spike, a mixture of ^{61}Ni-^{62}Ni isotopes ($^{60}Ni/^{58}Ni = 0.732349$; $^{61}Ni/^{58}Ni = 48.797310$; $^{62}Ni/^{58}Ni = 44.346698$), was added to each sample with a Ni sample/spike ratio of 1 prior to chemical separation through Ni-spec resin. Application of a three-dimensional data reduction procedure was used to determining the true isotope ratios of the samples (Siebert et al., 2001). Nickel isotope compositions are reported in delta notation $\delta^{60/58}Ni$ (per mil) relatively to the Ni isotopic standard NIST SRM 986 (1):

$$\delta^{60/58}Ni = (^{60}Ni/^{58}Ni_{sample}/^{60}Ni/^{58}Ni_{NIST986} - 1) \times 1000 \qquad (1)$$

Internal precision on Ni isotope delta values are determined as a two-standard error of the mean (2se) calculated with the 50 run cycles used for double-spike calculations (Gueguen et al., 2013) and is typically comprised between 0.03 and 0.04 ‰. External precision, determined by duplicate of digested and purified geological reference materials (Nod-A-1, Nod-P-1) and replicate of analysis of these materials on the mass spectrometer is determined at 0.04 ‰ (2sd; n=7; Table 1d) with $\delta^{60/58}Ni$ values of 1.06 ‰ and 0.34 ‰ respectively. Error bars reported in the figures correspond to the external precision.

199 *2.4. Beryllium isotope analysis*

200

201 Selected Fe-Mn crusts sub-samples were analyzed for $^{10}Be/^{9}Be$ ratio by Accelerator
202 Mass Spectrometry (AMS ASTER) at CEREGE (Aix-en-Provence, France) using previously
203 established methods (Bourles et al., 1989; Lebatard et al., 2008; Arnold et al., 2010). In short,
204 collection of Be was made using a leaching method which consists in a chemical extraction of
205 Be from its matrix using 0.04 M NH_2OH-HCl and 25% acetic acid. An aliquot of each sample
206 was measured for ^{9}Be concentrations by graphite furnace atomic adsorption
207 spectrophotometry (GFAAS, Hitachi Z8200). The remaining of the sample was spiked with
208 ^{9}Be, and the total Be was purified using solvent extraction methods and then transformed to
209 BeO for mass spectrometry analysis. ^{10}Be concentrations were calculated from the measured
210 spiked $^{10}Be/^{9}Be$ ratios and the true $^{10}Be/^{9}Be$ ratio of the sample was calculated using ^{9}Be
211 measured by GFAAS and ^{10}Be measured by AMS. The precision for each sample analysis
212 was determined on repeated measurements (n=4) of the sample and the final uncertainty
213 calculated on the $^{10}Be/^{9}Be$ ratio was generally better than 5%.

214

215 **3. Results**

216

217 *3.1. Elemental geochemistry*

218 *3.1.1. North Pacific Fe-Mn crusts from Apuupuu Seamount*

219 Elemental concentrations and selected elemental ratios are reported in Table 1.
220 Average Mn concentrations are ~14-15 wt%, whereas Fe contents are ~10 wt%. Transition
221 metal concentrations are in the range of ~910 to 4,700 µg/g for Co, Cu and Zn concentrations
222 yield average values of ~1,000 and ~600 µg/g respectively, and the average Ni concentrations
223 vary between ~2,100 and 3,000 µg/g for J2-480 and J2-480-R14, respectively. Beryllium

concentrations are homogenous in the range of 4.3 to 6.2 µg/g in J2-480 and 3.5 to 5.0 µg/g in J2-480-R14. Elements suggestive of authigenic enrichment of phosphatic minerals such as P yield average values of ~25,000 and ~2,400 µg/g for J2-480 and J2-480-R14 respectively. In general, hydrogenetic Fe-Mn crusts display a perfect correlation between P and Ca concentrations, which is likely related to the fact that these two elements are essentially hosted in authigenic phosphatic phases. This is consistent with higher Ca concentrations of 54,000 µg/g obtained for J2-480 in comparison to Ca contents of ~13,000 µg/g measured for J2-480-R14. Lithogenic elements such as Al and Ti have similar concentrations for the two North Pacific Fe-Mn crusts with values of ~4,000 µg/g and ~7,700 µg/g respectively.

Although all samples fall in the hydrogenetic field in the ternary diagram (Figure 3) of Bonatti et al. (1972), it should be noted that the bottom of crust J2-480 tends towards the hydrothermal field due to higher Fe concentrations and lower Mn, Ni, Cu and Co concentrations. As reported in other studies, the concentration patterns of, Ni, Co, and Cu tend to covary with Mn concentrations (Koschinsky and Halbach, 1995; Koschinsky and Hein, 2003) suggesting that the Mn-phase controls the distribution and enrichment of these metals in the crust. Therefore, we also normalized transition metal concentrations to Mn in order to avoid possible dilution effects due to the presence of other phases (e.g., phosphates, silicates, Fe-oxyhydroxides). When normalized to Mn concentrations, contents of metals such as Cu, Ni, Co, and Zn to a lesser extent show an increase below ~15 mm in crust J2-480 and below ~9 mm in crust J2-480-R14 (Figure 4). Fe/Mn ratios determined for each growth layer range from 0.45 to 1.46 (g/g) (Table 1) which is typical of values already reported for other hydrogenetic Fe-Mn crusts from the North and Central Pacific Ocean (Halbach et al., 1983; De Carlo et al., 1987; Hein et al., 1988; Puteanus and Halbach, 1988; Koschinsky and Halbach, 1995; Koschinsky et al., 1997; Frank et al., 1999; Hein et al., 2013; Hein and Koschinsky, 2014). In general, compositional variations of transition metals are more

pronounced in J2-480 than in J2-480-R14 (Figure 4). Fe/Mn ratios increase in J2-480 at ~15 mm depth from ~0.60 to ~1.40 whereas it remains stable in J2-480-R14. Al/Fe ratios, which are used as an estimate of the lithogenic contributions, vary between 0.03 and 0.06 in crust J2-480-R14. These variations, however, are not specifically correlated with other metals concentrations. By contrast, Al/Fe sharply increases in J2-480 crust from ~15 mm depth towards the bottom from 0.03 to 0.15 which also corresponds to the increase in other transition metals such as Cu, Ni and Co (Figures 4 and 6).

3.1.2. South Pacific Fe-Mn crusts from French Polynesia

South Pacific Fe-Mn crusts have lower Mn concentrations (average Mn ~9-10 wt%) than North Pacific Fe-Mn crusts and they also have lower Fe contents (average Fe ~8 wt%) (Table 1). Average Co concentrations range between ~ 4,800 and 5,400 µg/g, while other transition metals like Cu and Zn show average concentrations of ~500 and ~300 µg/g respectively. Ni concentrations are on average comprised between ~1,200 and 2,000 µg/g. Beryllium concentrations are in general lower than in North Pacific Fe-Mn crusts and vary between 1.4 to 4.1 µg/g in ZEP2-DR05-04 and between 2.0 and 3.1 in ZEP2-DR-06-03. The two Fe-Mn crusts display distinct average Ca concentrations, i.e. ~14,000 µg/g in ZEP2-DR05-04 and 44,000 µg/g in ZEP2-DR06-03. Calcium concentrations are in agreement with distinct P concentrations observed between the two Fe-Mn crusts, where P concentrations in ZEP2-DR05-04 are ~3,600 µg/g on average and ~7,700 µg/g in ZEP2-DR06-03. The latter displays a 10-fold increase in Ca and P concentrations from the surface of the crust to the base of the crust, i.e., from ~12,000 µg/g to ~120,000 µg/g for Ca and from ~2,900 µg/g to ~31,000 µg/g for P, with a steep increase from ~12 mm and ~23 mm depth in the crust. This suggests significant phosphatization in ZEP2-DR06-03. Finally, we found similar ranges of

Al and Ti concentrations than for North Pacific Fe-Mn crusts of ~4,000 µg/g and ~2,700 µg/g respectively.

The range of Fe/Mn ratios from 0.53 and 1.31 in the South Pacific Fe-Mn crusts are similar to the ratios measured in North Pacific Fe-Mn crusts and they are also in the range of Fe/Mn ratios reported for other South Pacific Fe-Mn crusts (Frank et al., 1999; Hein et al., 2013). All subsamples of the two Fe-Mn crust profiles fall in the hydrogenetic field (Figure 3) of the Bonatti et al. (1972) diagram. However, differences between North and South Pacific Fe-Mn crusts are observed in terms of enrichment factors between each crust such that Co enrichment, i.e., Co/Mn ratios, are higher (Co/Mn>0.04) in South Pacific Fe-Mn crusts than for in North Pacific Fe-Mn crusts (Co/Mn~0.02; Figure 5 and Table 1). In addition, we distinguished two distinct regions, “I” and “O”, in ZEP2-DR05-04 crust since they display significant geochemical differences (Figure 4). Region “O” is between 0.5 mm (top) to 16.5 mm depth in the crust, and region “I” includes layers from 17.5 mm to 22 mm depth (i.e., over a thickness of ~4 mm at the bottom of the crust). The region “I” shows a two-fold difference in Ni and Cu concentrations compared to the region "O" (Figure 4). Other layers in the crust show remarkably similar geochemical patterns, in particular with respect to Cu/Mn, Co/Mn, Ni/Mn and Fe/Mn ratios. Ni/Mn ratios vary around an average value of 0.15, while Zn/Mn and Cu/Mn ratios are slightly decreasing from bottom to top of the crusts (i.e., from ~0.002 to 0.040 for Zn/Mn and from ~0.002 to 0.060 for Cu/Mn). Co/Mn ratios decrease from about 0.075 to 0.04 in the first 5-10 mm of the crust, and remain relatively constant at ~0.05 from 10 to 25 mm. This possibly indicates a decrease in growth rates of the crusts. Aluminum enrichment relative to Fe is different between the two crusts, ZEP2-DR06-03 crust displays constant Al/Fe ratio from 10 mm depth towards the bottom of the crust with values ~0.050, while it decreases from 10 mm depth to the top of the crust to values up to 0.026. These values are well below the average Al/Fe ratio of the Upper Continental Crust of 3.06

(Rudnick and Gao, 2014) consistent with a limited detrital component in Fe-Mn crusts. ZEP2-DR05-04 crust shows constant Al/Fe ratios centered ~0.040, but significantly increase up to 0.112 from 17.5 mm depth towards the bottom of the crust. The shift is concomitant to the increase in Ni/Mn, Cu/Mn and Zn/Mn ratios.

3.2. Fe-Mn crust dating and calculation of growth rates using Be isotope ratios

A common method for dating Fe-Mn crusts has involved the measurement of the cosmogenic isotope ^{10}Be (Tanaka and Inoue, 1979; Segl et al., 1984; Bourles et al., 1989; Morris, 1991; Ling et al., 1997; Frank et al., 1999; Frank et al., 2002; Ling et al., 2005; Amend et al., 2011). Although the Co-dating method (i.e., Co enrichment in the crust) has been used in the past (e.g., Halbach et al., 1983), it could yield inaccurate ages in the case of variable Co fluxes to the oceans (Kyte et al., 1993). The Be dating method is based on the assumption that ^{10}Be is supplied at a constant rate to the oceans, so that ^{10}Be/^{9}Be ratios should be uniform in the surface layer of Fe-Mn crusts (Ku et al., 1990; von Blanckenburg et al., 1996a; Willenbring and von Blanckenburg, 2010a). The advantage of this method is the determination of an absolute age of Fe-Mn crust, which is not affected by possible hiatuses during crust growth. Since ^{10}Be has a short half-life of 1.39 Ma (Willenbring and von Blanckenburg, 2010a), this method can only be used for dating Fe-Mn crusts up to ~20 Ma. Hence, we measured ^{10}Be/^{9}Be ratios only for the top 2.5 cm of each crust. We calculated absolute ages of subsamples using an initial ^{10}Be/^{9}Be ratio of 1.1×10^{-7} (von Blanckenburg et al., 1996a) and a λ value of 0.498667036 myr^{-1} for ^{10}Be (Table 2).

^{10}Be/^{9}Be ratios in J2-480 range from 3.14×10^{-9} at the top of the crust to 2.71×10^{-10} towards the bottom of the crust (Table 2 and Figure 5). A larger range is observed for J2-480-R14 from 1.75×10^{-8} at the top of the crust to 2.31×10^{-11} towards the bottom. Results for J2-

480-R14 crust show near linear decrease of Ln(^{10}Be/^{9}Be) with crust depth suggesting constant growth rate, at least for the top 18 mm of the crust (Figure 5) which was estimated at 1.1 ±0.5 mm/Ma. Precise dating of sample J2-480 is impaired by the limited subsampling intervals (only 3 data points) but an average growth rate of 1.6 mm/Ma was determined. From the top to bottom layer, J2-480 and J2-480-R14 crust sections span an age from 7.1 to 12.0 Ma and 3.7 to 17.0 Ma respectively. The results suggest that both Fe-Mn crusts from Apuupuu Seamount have similar average growth rates, consistent with similar Co/Mn ratios of 0.021 ± 0.01 and 0.031 ± 0.01 respectively. A striking result of ^{10}Be dating is that the uppermost layer of the crusts does not show "zero" ages as expected. Possible explanations are either that Fe-Mn crusts J2-480 and J2-480-R14 stopped growing some millions years ago (i.e., presence of hiatuses), or that the top part of the crusts was broken and was not recovered during the sampling process. The lack of significant Co enrichment in the uppermost layers compared to other section of the crusts argues against an abrupt decrease in growth rates. Using the average growth rates obtained for each crust, the estimated thickness of the uppermost crust layers that appear missing is about 11 mm for J2-480 and 4 mm for J2-480-R14. Hence, it is possible that the first centimeters of the crust layers were lost during sampling, probably due to the difficulty to recover these samples from smooth surface of bare rocks using the articulated arm of the ROV (Figure 2).

^{10}Be/^{9}Be ratios from 6.91×10^{-8} to 3.51×10^{-9} are observed in ZEP2-DR06-03 crust with decreasing values from top to bottom of the crust. ZEP2-DR05-04 crust shows a different pattern where Be isotopes do not follow the expected trend if radioactive decay is the only controlling factor. In this sample, ^{10}Be/^{9}Be ratios range from 1.40×10^{-7} at about 17.5 mm from top, 1.02×10^{-8} at ~0.5 mm and 6.50×10^{-9} at 12.5 mm (Table 2 and Figure 5). Hence, ZEP2-DR05-04 crust displays anomalously high ^{10}Be/^{9}Be ratios in the bottom, i.e., older part of the crust (Figure 5). In particular, ^{10}Be/^{9}Be ration of 1.4. 10^{-7} measured at 17.5 mm is similar,

albeit slightly higher, than the present-day $^{10}Be/^{9}Be$ ratio in seawater. Potential reasons for the aberrant youth of the crust are discussed in more details below. We cautiously avoided using the $^{10}Be/^{9}Be$ data to provide age estimates for ZEP2-DR05-04.

Layers of ZEP2-DR-06-03 can be divided into two parts in terms of growth rates. The upper half crust from depth to 0.5 to ~13 mm depth is characterized by an average growth rate estimated at 1.7 ± 0.6 mm/Ma, while the second half part of the crust corresponding to depths between ~13 mm and 23.5 mm has an average higher growth rate of 3.2 ± 0.6 mm/Ma. The variations in growth rates is consistent with the increase in Co/Mn ratios from ~13 mm to 0.5 mm depth in the crust (Figure 5) suggesting enrichment in Co concentrations due to lower growth rates. These growth rates are generally in the range reported in the literature for hydrogenetic Fe-Mn deposits (Frank et al., 1999; Frank, 2002). The time periods spanned by ZEP2-DR06-03 subsamples is between 0.9 and 6.9 Ma.

Considering the very similar profile in Co/Mn ratios obtained in crusts ZEP2-DR05-04 and ZEP2-DR06-03 (Figure 5), including the "kink" at ~5 mm depth, we consider that both crusts have on average similar growth rates.

3.3. Ni isotope ratios

Nickel isotope compositions for North Pacific Fe-Mn crusts subsamples are rather uniform in the range of 1.64 to 1.72 ‰ for crust J2-480 with the exception of the most basal point at 19 mm depth yielding a $\delta^{60/58}$Ni value of +1.41 ‰. Sample J2-480-R14 displays variations from 1.70 to 1.86 ‰ with the exception of the top of J2-480-R14 at 0.2 mm depth, which has a heavier $\delta^{60/58}$Ni of 1.94 ‰ (Figure 6 and Table 2). Average values are 1.65 ±0.19 ‰ (2sd) and 1.79 ±0.13 ‰ (2sd) for J2-480 and J2-480-R14 respectively, and although the observed variations exceed the reproducibility of the measurements (i.e., ±0,04 ‰) the range

374 falls within the range of previously published data (Gall et al., 2013). Nickel isotope
375 compositions of South Pacific Fe-Mn crusts subsamples vary from 1.75 to 1.95 ‰ in ZEP2-
376 DR06-03 crust with an average value of 1.87 ±0.10 ‰ (2sd, n=14). In ZEP2-DR05-04 crust,
377 the "I" region of the crust show a significant variability in $\delta^{60/58}$Ni values from 0.25 to 1.08 ‰
378 with lowest values at the bottom of the crust in contact with the substrate. In contrast, $\delta^{60/58}$Ni
379 values in the "O" region are comprised between 1.54 to 1.86 ‰ with an average value of 1.72
380 ±0.18 ‰ (Table 2 and Figure 6). Light Ni isotope compositions correlates with low Mn/Ni
381 ratios (R^2=0.99 for the last five samples at the bottom of the crust; Figure 7D). With the
382 exception of the inner region "I" of ZEP2-DR05-04 crust, both range of values in the South
383 Pacific Fe-Mn crusts are similar to North Pacific Fe-Mn crusts.
384
385 **4. Discussion**
386
387 *4.1. Mechanisms of Ni incorporation into Fe-Mn crusts and Ni isotope variability of Fe-Mn*
388 *crusts surfaces*
389
390 Nickel isotope composition of surface layers of hydrogenetic Fe-Mn crusts scrapings
391 from various localities previously reported by Gall et al. (2013) shows a range from 0.9 to 2.5
392 ‰ with an average value of 1.62 ±0.78 ‰, which indicates both lighter and heavier values
393 than the average Ni isotope composition of seawater of 1.44 ±0.15‰ (Cameron and Vance,
394 2014). However, it is important to recall that even surface scrapings of Fe-Mn crusts do not
395 exactly represent an instantaneous picture of ambient seawater. Considering average growth
396 rates between 1 to 5 mm/Ma typical for Fe-Mn crusts, precise sampling (i.e., scraping) of the
397 first 0.1 to 0.5 mm of Fe-Mn crust yield ages ranging from 0.5 Ma to not less than 20 ka.

Hence, the time resolution is significantly longer than the estimated residence time of Ni in the ocean and it is possible that Ni isotope composition in seawater changed during that time.

Gall et al. (2013) observed that the surface scrapings of Fe-Mn crusts formed close to continental margins yielded heavier $\delta^{60/58}$Ni values up to 2.5 ‰ which could be attributed to a higher contribution of input materials from continental weathering (e.g., rivers and groundwaters). The authors also discussed the effect of deep ocean water redox state and showed that no correlation could be established between oxygen saturation state and Ni isotope variations. In this study, we obtained a single $\delta^{60/58}$Ni value of 1.88 ±0.04‰ for crust layers younger than 0.9 Ma (i.e., sample ZEP2-DR06-03-L1). This value is remarkably similar to the average value of the crust for the last 7 Ma (Tables 1 and 2), suggesting that seawater Ni isotope values as recorded in Fe-Mn crusts remained relatively constant. By comparison, Gall et al. (2013) obtained lighter $\delta^{60/58}$Ni value at 1.04 ± 0.25 ‰ (2sd) for the surface scraping of a Fe-Mn crust recovered about 400 km westward (Fe-Mn crust SO-36, 22°21'S, 150°17'W) of the studied ZEP2-DR06-03 Fe-Mn crust. Both values are different from modern seawater estimated at 1.44 ±0.15 ‰ (Cameron and Vance, 2014).

Recent experimental work has shown relatively large Ni isotope fractionation during Ni sorption to Fe-oxyhydroxides (Gueguen et al., 2011; Sorensen et al., 2011; Gueguen, 2013; Wasylenki et al., 2015) and Mn-oxyhydroxides (Gueguen, 2013; Wasylenki et al., 2014a) with preferential uptake of isotopically light Ni on the mineral surface. Results on natural samples show that to a first approximation the enrichment in the heavy Ni isotopes in the surface layer of Fe-Mn crusts relative to seawater (1.88 ±0.10 ‰ vs 1.44 ±0.15 ‰) is at odds with experimental studies showing preferential enrichment in light Ni isotopes on Mn-oxides surface (e.g., birnessite) by up to -2.5 ‰ (Gueguen, 2013; Wasylenki et al., 2014a). Enrichment in heavy Ni isotopes for surface scrapings ($\delta^{60/58}$Ni value up to 2.00 ± 0.05 ‰) has been also reported elsewhere in the South or North Central Pacific (Gall et al., 2013). This

423 suggests either that another mechanism rather than adsorption reactions is responsible for
424 heavy isotope fractionation during Ni uptake in Fe-Mn crusts or that seawater changed rapidly
425 within the last 1 Ma. We discuss below possible mechanisms explaining both heavier and
426 lighter Ni isotope composition in Fe-Mn crusts relative to seawater.

427 Ferromanganese crusts are formed through the slow precipitation of Fe-Mn colloids,
428 initially formed in seawater, on a hard substrate devoid of sediments (Koschinsky and
429 Halbach, 1995). Metal cations, such as Ni are readily coprecipitated with Fe-Mn colloids and
430 can undergo further precipitation through slow uptake (i.e., adsorption) onto Fe-Mn crust
431 surface. Hence, even if the removal of Ni onto Fe-Mn colloids in the water column is
432 relatively rapid, which should result in significant Ni isotope fractionation, most of Ni
433 adsorption occurs directly on the crust surface. EXAFS results on experimental Ni adsorption
434 on birnessite at neutral pH indicate that adsorbed Ni is structurally incorporated within the
435 mineral with time, e.g., 30% of Ni is incorporated within 408 hours (Peacock, 2009). Thus, it
436 is possible that adsorbed Ni on Fe-Mn crust surface is continuously incorporated in the
437 mineral structure as a result of long exposure of the crust surface to seawater. This process
438 would allow isotopic exchange of Ni with seawater and any potential isotope fractionation
439 that would have initially occurred during adsorption reactions would not necessarily be
440 recorded in the final product of the reaction. In support of this hypothesis, the experimental
441 study of Cd isotope fractionation during adsorption of Cd on birnessite in high ionic strength
442 solution (i.e., artificial seawater) indicated that the isotope fractionation factor between
443 dissolved Cd and adsorbed Cd decreases with time, from 0.4 ‰ at the beginning of
444 experiment to 0.1 ‰ after 912 hours (Wasylenki et al., 2014b). The final Cd isotope
445 fractionation factor ~0.1 ‰ was similar to the isotope fractionation of Cd observed during
446 experiments in low ionic strength solution and that measured between seawater and Fe-Mn
447 crusts (Schmitt et al., 2009; Horner et al., 2010). The experimental data suggest, therefore, a

448 reversible mechanism during exchange of dissolved Cd and adsorbed Cd in high ionic
449 strength conditions. It is possible that a similar mechanism explains the range of Ni isotope
450 composition in Fe-Mn crusts, that is, the structural incorporation of Ni within the crust with
451 time favors the heavy Ni isotopes while initial adsorption of Ni onto Fe-Mn minerals favors
452 the light Ni isotopes.

453 It has been shown that Ni speciation in seawater is dominated by aqueous Ni^{2+} and Ni-
454 chloro complexes (Bruland, 1980; Bruland, 1983; Bruland et al., 1994; Fujii et al., 2011), as
455 well as organically-bound species (Van Den Berg and Nimmo, 1987; Nimmo et al., 1989;
456 Turner et al., 1998). In addition, experimental and theoretical results indicate that Ni isotopes
457 are prone to large fractionation up to ~2.5 ‰ between isotopically heavy inorganic and
458 isotopically light organic Ni species in seawater (Fujii et al., 2011), which demonstrates that
459 Ni speciation in the water column may also affect Ni isotope composition of Fe-Mn crusts. In
460 the case of the preferential adsorption of aqueous Ni^{2+} species on Mn-oxides colloids relative
461 to isotopically light organic species (e.g., Nickel carboxylate complexes; Fujii et al., 2011),
462 the expected enrichment in light Ni isotopes during adsorption will be muted by the inverse
463 fractionation between inorganic and organic Ni species in solution. In similar manner, Little et
464 al. (2014b) interpreted heavier Zn isotope compositions of Fe-Mn crusts relative to seawater
465 as the result of fractionation between free aqueous Zn^{2+} (preferentially adsorbed on Fe-Mn
466 crusts) and Zn chloro-complexes, the latter being predicted to favor light Zn isotopes. Because
467 free Ni^{2+} and Ni-chloro complexes are also the predominant species occurring in seawater
468 (Fujii et al., 2011), with Ni-chloro complexes being enriched in light Ni isotopes compared to
469 aqueous Ni^{2+} (Fujii et al., 2011), similar mechanisms could affect both Ni and Zn isotopes in
470 Fe-Mn crusts. However, although Ni speciation certainly plays an important role in the
471 fractionation of Ni isotopes between Fe-Mn crusts and seawater, it is unlikely that the relative
472 abundance of free Ni^{2+} and Ni-chloro complexes is variable in seawater. Hence, Ni speciation

473 in seawater is unlikely to explain the range of Ni isotopes in Fe-Mn crusts within oceanic
474 basins. Processes involving the pathways of Ni incorporation in Fe-Mn crusts therefore
475 provide the most plausible mechanisms, together with post-depositional effects as discussed
476 in the following section 4.2.
477
478 *4.2. Evidence for diagenetic alteration and post-depositional effects in Fe-Mn crusts and the*
479 *response of Ni isotopes to late-stage alteration*
480
481 The high $^{10}Be/^{9}Be$ ratios in the region "I" of ZEP2–DR05–04 crust (Table 2 and
482 Figures 5) is at odds with the general assumption that Fe-Mn crusts are composed of Fe-Mn
483 oxides layers that accumulated successively through time onto a hard substrate, implying that
484 $^{10}Be/^{9}Be$ ratios in the crust profile should decrease from top to bottom. The inner region "I" of
485 this crust also corresponds to the region where important geochemical variability is observed,
486 in particular with respect to Mn, Fe, Ni, and Cu concentrations. There is an increase in
487 Cu/Mn, Ni/Mn, Zn/Mn and Al/Fe ratios at the bottom of ZEP2-DR05-04 while Co/Mn ratios
488 remain similar to the other crust ZEP2-DR06-03 recovered from the same area. In the outer
489 region "O" of the crust, Cu/Mn, Fe/Mn and Zn/Mn are remarkably similar between both
490 crusts. This suggests that growth rates or water mass parameters are not the major controls on
491 the enrichment in Ni and other transition metals in crust ZEP2-DR05-04. Below, we consider
492 three possible explanations that may account for the anomalously high $^{10}Be/^{9}Be$ ratios and
493 associated geochemical variations: (1) unusually high initial $^{10}Be/^{9}Be$ ratios; (2) diffusion
494 processes; (3) phosphatization effects; and (4) protracted seawater circulation throughout the
495 base of the crust in contact with the substrate.
496 Hypothesis (1): most of the flux of cosmogenic ^{10}Be to the ocean has an atmospheric
497 origin and is directly related to the flux of the incoming cosmic ray particles (Willenbring and

von Blanckenburg (2010b, 2010a); Steinhilber et al. (2012) and references therein). Although variations in geomagnetic field strength and changes in solar modulation produce fluctuations in ^{10}Be flux, it remained roughly constant over the last 12 Ma (Willenbring and von Blanckenburg, 2010b). ^{9}Be fluxes to the ocean, mainly derived from fluvial inputs also remained constant, precluding a change of initial $^{10}Be/^{9}Be$ ratios during the formation of the crusts. In addition, ^{9}Be concentrations are relatively constant through the Fe-Mn crust layers (Table 2), suggesting that unusual high $^{10}Be/^{9}Be$ ratios are not the results of ^{9}Be depletion. Although cosmic spherules have been already reported in Fe-Mn crusts (e.g., Kosakevitch, 1987; Halbach et al., 1989), high initial $^{10}Be/^{9}Be$ ratios are unlikely to originate from the presence of meteoritic particles with high ^{10}Be content since cosmic particles yield ^{10}Be below 0.17 pg/g (Nishiizumi et al., 1991). Stuart and Lee (2012) detected the presence of micrometeorites using He isotopic composition of Fe-Mn crusts, however their Fe-Mn crust was dated using cosmogenic ^{10}Be isotope implying that extraterrestrial inputs have not modified the $^{10}Be/^{9}Be$ ratios of Fe-Mn crust. Hence, the presence of extraterrestrial material is probably not the cause of elevated $^{10}Be/^{9}Be$ isotope ratios, and probably also elevated Ni/Mn ratios in our sample.

Hypothesis (2) can also be disregarded since it was demonstrated that on the time-scale considered for dating Fe-Mn crusts diffusion of Be is very limited (Henderson and Burton, 1999). If diffusion processes affect Be in the crust, it could modify the isotopic pattern showing decreasing values from top (young crust) to the bottom (old crust) and skewed the age model based on $^{10}Be/^{9}Be$ isotope ratios.

Hypothesis (3): the presence of accessory phases such as fluorapatite and calcite generally indicates alteration processes in the Fe-Mn crust with possible remobilization of transition metals in the crust. This effect, known as phosphatization, has been described in some Pacific Fe-Mn crusts (Halbach and Puteanus, 1984; Hein et al., 1993). Phosphorus and

calcium in Fe-Mn crusts are essentially hosted in accessory fluorapatite and calcite phases, with minor contribution from detrital materials and their concentrations vary in our Fe-Mn crusts, in particular crust ZEP2-DR06-03 (Table 1). However, variations in P concentrations are not correlated with any variations in transition metal concentrations nor with isotopic variations (Figure 7), suggesting that phosphatization effects can be discounted for explaining the compositional variability in our Fe-Mn crusts. More specifically, the bottom of crust ZEP2-DR05-04 (with anomalous $^{10}Be/^{9}Be$ ratios) does not show any specific trend in P concentrations (Figure 7) indicating that the crust did not undergo major phosphatization, which is thus unlikely to be the cause for the variations observed in other geochemical proxies. Finally, large P/Ni ratios also do not correlate with $\delta^{60/58}Ni$ values (Figure 7).

Finally, hypothesis (4) and the effect of post-depositional fluid circulation through the crust is likely the most plausible explanation for our observations. Several lines of evidence suggest that the region "I" of the crust has been affected by alteration processes. First, sample ZEP2-DR05-04 consists of 25 mm thick Fe-Mn crusts attached to a brecciated basalt substrate mixed with phosphorites and carbonates. Hence, it is possible that continuous circulation of fluids occurred through fractures from the underlying substrate. Fluid circulation would continuously bring seawater-derived Be with higher $^{10}Be/^{9}Be$ ratios (i.e., present-day $^{10}Be/^{9}Be$ ratio) thus producing the anomalous Be isotope composition in region "I" of the crust. Substantial alteration and reprecipitation of Mn-oxides phases at the expense of Fe-oxides would have also promoted the observed enrichment in transition metals such as Ni, Cu, Zn due to their high affinities towards the Mn-phase.

One of the most striking feature observed in ZEP2-DR05-04 crust is the fractionation of Ni isotopes towards lighter $\delta^{60/58}Ni$ values at the bottom of the crust from 1.06 to 0.25 ‰, which strongly correlate with the geochemical variations described above, in particular decreasing Mn/Ni ratios (Figure 7D). Four possible scenarios may account for such light Ni

548 isotope compositions, (1) lighter Ni isotope composition of ambient seawater at the time of
549 crust formation, (2) meteoritic or basaltic/detrital inputs, (3) hydrothermal or halmyrolitic
550 inputs (i.e., alteration of the substrate by fluids on the seafloor), and (4) alteration and
551 reprecipitation processes of Mn-oxide phases.

552 A primary isotopic signal acquired from local seawater for explaining lighter Ni
553 isotopes in the Fe-Mn crust would require either a change in the isotopic composition of local
554 sources of Ni or a change in the input and/or output fluxes of Ni in the oceans. A local source
555 would likely have affected the two Fe-Mn crusts collected at the same location, while a
556 change in the input and/or output fluxes in the oceans should have affected the four Fe-Mn
557 crusts collected in the same oceanic basin, i.e., the Pacific Ocean. Nonetheless, both
558 hypotheses are inconsistent with the Ni isotope composition of the three other Fe-Mn crusts,
559 which therefore rules out the possibility that light $\delta^{60/58}$Ni values in ZEP2-DR05-04 are a
560 primary signal from seawater.

561 Secondly, considering the ubiquitous occurrence of Fe-Ni cosmic spherules in South
562 Pacific Fe-Mn crusts (e.g., Kosakevitch, 1987; Halbach et al., 1989), the potential
563 contribution of meteoritic Ni should be evaluated. Nickel isotope compositions of iron
564 meteorites reported in previous studies yield a range of $\delta^{60/58}$Ni values from 0.24 and 0.36 ‰
565 (Moynier et al., 2007; Cook et al., 2008; Cameron et al., 2009; Gueguen et al., 2013).
566 However, iron meteorites such as Gibeon Iron (class IVA) and Nantan Iron (class IIICD) have
567 Ni/Fe ratios of about 0.07, which are similar to those obtained in the bottom section of crust
568 ZEP2-DR05-04. Hence, using simple mass balance considerations, it is unlikely that the entire
569 pool of Ni at the base of ZEP2-DR05-04 crust derived solely from meteoritic input.

570 As reported in Figure 7D, light $\delta^{60/58}$Ni values in ZEP2-DR05-04 crust correlate with
571 lower Mn/Ni ratios (R^2=0.99; for the 5 subsamples at the bottom of the crust), implying
572 possible mixing relationships between typical hydrogenous Ni end-member (Mn/Ni ~ 60;

573 $\delta^{60/58}$Ni ~ 1.8 ‰) and light $\delta^{60/58}$Ni values from the basaltic substrate (low Mn/Ni; $\delta^{60/58}$Ni ~ 0
574 ‰; (Gall et al., 2012; Gueguen et al., 2013). However, the presence of detrital or volcanic
575 material can be discounted for explaining geochemical variations in ZEP2-DR05-04 crust.
576 Although Ti along with Al is often used as an indicator of the presence of detrital phases and
577 silicate-rich material in marine sediments, Koschinsky and Halbach (1995) showed that a
578 large proportion of Ti in hydrogenetic Fe-Mn crusts is mainly derived from seawater as
579 colloidal Ti (i.e., uncharged Ti hydroxo-complexes adsorbed on the positively-charged Fe-
580 colloids) and is not controlled by detrital material. Addition of crustal material to the Fe-Mn
581 crust would have affected both Al and Ti enrichment in the crust in similar manners. Al/Fe
582 ratios are constant in ZEP2-DR05-04 crust while Ti/Al ratios decrease in the altered portion
583 of the crust (Table 1). The latter would be consistent with alteration of Fe-phases and loss of
584 Ti hosted in the Fe-phase to the fluid, implying that crustal Ni is unlikely to be the cause for
585 light $\delta^{60/58}$Ni values.

586 The third scenario, involving halmyrolitic reactions could potentially reconcile
587 isotopically light Ni isotopes, low Mn/Ni ratios and anomalous Be isotope ratios.
588 Halmyrolysis has been described in volcanic context and is defined as low temperature
589 alteration of volcanic material by seawater (Staudigel and Hart, 1983; Staudigel et al., 1996).
590 Although limited data are available on Ni isotope fractionation during alteration of volcanic
591 rocks, preliminary study has shown that fresh and altered basalts have the same $\delta^{60/58}$Ni values
592 (Gueguen et al., 2013). In contrast, continental weathering of ultramafic complexes on land
593 has been shown to produce light Ni isotope enrichment in laterites, leading to preferential loss
594 of heavy Ni isotopes in the dissolved phase (Ratié et al., 2015), consistent with light Ni
595 isotopes being retained in Fe-oxides (Wasylenki et al., 2014b). Based on these results, one
596 should expect that halmyrolytic processes would promote the release of a non-fractionated to
597 heavy Ni isotope signature in the alteration fluids (i.e., relative to fresh basalt), which is not

598 consistent with the light (i.e., near-zero) $\delta^{60/58}$Ni values observed in ZEP2-DR05-04 crust. As
599 discussed in Gall et al. (2013), lighter $\delta^{60/58}$Ni values down to 0.9 ‰ were interpreted as
600 reflecting hydrothermal inputs of Ni, although no distinction was mentioned between low or
601 high-temperature processes. It is important to note however, that significant hydrothermal
602 inputs in Fe-Mn crusts would have increased Fe/Mn ratios (i.e., Chu et al., 2006) while adding
603 isotopically light Ni (i.e., near crustal values). This would have also resulted in significant
604 dilution of other transition metals, in particular Co (Manheim and Lanebostwick, 1988),
605 which is not observed here. Hence, we do not favor a potential hydrothermal or halmyrolitic
606 origin for the enrichment of Ni in this crust.

607 Finally, the fourth possible and favored scenario for explaining Ni isotope
608 fractionation is the effect of post-depositional alteration and reprecipitation of Mn-oxide
609 phases of the crust. Preliminary results suggest significant Ni isotope fractionation during Ni
610 sorption on Mn-oxides (e.g., birnessite; Gueguen, 2013; Wasylenki et al., 2014a). Data from
611 ZEP2-DR05-04 crust indicate large light Ni isotope fractionation towards light values (from
612 1.08 to 0.25 ‰), supporting the assumption that Ni sorption to Mn-oxides surfaces in natural
613 deposits also fractionates Ni isotopes. Hence, our observations demonstrate that Ni sorption
614 on Mn-oxides is a fundamental process controlling Ni isotope fractionation in the natural
615 environment. Here, we propose that Mn-oxide alteration involving dissolution and
616 reprecipitation could explain Ni isotope variations without necessarily involving additional
617 inputs of Ni or change of seawater composition. The sharp increase in Ni/Mn ratios (Figure 4)
618 without a concomitant decrease in Co/Mn ratios in region "I" of the crust (Figure 5) argue
619 against an initial rapid precipitation of Mn-oxides from seawater during formation of the
620 crust, and therefore hydrothermal input which would have resulted in lowering Co/Mn ratios
621 (Manheim and Lanebostwick, 1988). In addition, $\delta^{60/58}$Ni values are not correlated with
622 Co/Mn ratios (Figure 7). The strong enrichment in Ni may be explained by a two-step model,

623 by which Ni is first adsorbed or incorporated in primary Mn-oxides phases, then release in
624 porewater during the alteration stage and then reprecipitated in open system. In this case, the
625 full expression of Ni isotope (i.e., probably more than 1.1 ‰ relative to seawater, which is
626 still lower than experimental values of > 2 ‰; Gueguen, 2013; Wasylenki et al., 2014a) is
627 recorded in the crust resulting in unexpectedly light $\delta^{60/58}$Ni values compared to the average
628 value of the Fe-Mn crust (~1.8 ‰). This scenario is also consistent with ^{10}Be/^{9}Be ratios since
629 abnormal values are also probably the result of re-equilibration with surrounding seawater or
630 alteration fluids (i.e., open system reprecipitation).

631 In summary, we interpret the light Ni isotope compositions of crust ZEP2-DR05-04 as
632 the result of fractionation from a source having a Ni isotope composition akin to that of
633 seawater, i.e., ~ 1.4 ‰ (Cameron and Vance, 2014), during adsorption reactions and late-
634 stage alteration processes. We consider sorption processes as being important drivers of Ni
635 isotope variations in Fe-Mn crusts, in addition to varying Ni isotope composition in seawater.
636
637 *4.3. Temporal Ni isotopes record in Fe-Mn crusts and implications for paleoceanography*
638
639 Prior to interpreting Ni isotope profile in Fe-Mn crust, it is crucial to first assess the
640 effect of diffusion processes, which could explain the homogenous Ni isotope composition in
641 Fe-Mn crusts. *In-situ* diffusion rate of Ni along the whole section of the crust can be
642 determined according to the equations from Henderson and Burton (1999). The distribution
643 coefficient of a given element is calculated as of the concentration in the surface of the crust
644 and in seawater, which is then compared with the diffusivity and the distribution coefficient of
645 uranium ($D^{X}_{eff} = (D^{U}_{eff}K^{U}_{crust})/K^{X}_{crust}$, where D_{eff} are the effective diffusivities and K_{crust} are
646 the distribution coefficients of element X and uranium (U)). Using this approach, we obtain a
647 diffusion rate on the order of ~10^{-9} cm^2/year which is slow enough compared to crust growth

rate so we can reasonably assume that Ni does not diffuse in Fe-Mn crusts. Hence, diffusion processes will not disturb Ni isotope composition in Fe-Mn crusts and pristine isotope composition should be preserved at the sampling scale carried out in this study.

Although the concentration of Ni varies in the water column due to its nutrient-type behavior, the relatively long oceanic residence time of Ni of ~10-30,000 yrs (Sclater et al., 1976; Bruland and Lohan, 2003; Gall et al., 2013; Cameron and Vance, 2014) in comparison to the ~1,500 yrs mixing time of oceans, likely implies that Ni distribution in deep waters is relatively well-mixed and homogenous. Nickel isotope profiles in the Pacific, Atlantic and Southern Ocean water columns do not show any variations with depth (Cameron and Vance, 2014), thus we can reasonably presume that Ni isotopes are homogenous in deep waters. At steady state, the Ni isotope composition of seawater is controlled by the relative fluxes of Ni inputs to the ocean (e.g., rivers, atmospheric deposits, hydrothermal sources) and Ni uptake (e.g., authigenic sinks, organic matter burial). The riverine flux and the authigenic sink (i.e., Ni scavenged in Mn-oxides phases) are respectively the main input and output fluxes of Ni in the ocean (Gall et al., 2013; Cameron and Vance, 2014), implying that the modern marine Ni isotope mass balance is controlled by the isotopic composition of these fluxes. Considering the relatively long residence time of Ni in the deep ocean, changes of either Ni input or output should have been recorded in both South and North Pacific crusts. In contrast, one may presume that different Ni isotope records between Fe-Mn crusts from the same oceanic basin would reflect either local sources, changes of Ni isotope fractionation factor between seawater and Fe-Mn crusts or post-depositional processes.

With the exception of the lower section of the crust ZEP2-DR05-04 which we argue is the result of post-depositional alteration processes (see the previous section 4.2), our results show fairly homogenous Ni isotope compositions in Pacific Fe-Mn crusts over the last ca. 17 Ma (Figure 6). We obtained, within uncertainties, similar average $\delta^{60/58}$Ni values of 1.72

673 ±0.18 ‰ (2sd) and 1.87 ±0.10 ‰ (2sd) in the South Pacific, and 1.65 ±0.19 ‰ (2sd) and 1.79
674 ±0.13 ‰ (2sd) in the North Pacific, thus confirming limited Ni isotope variations over the last
675 17 Ma and between different locations in the Pacific Ocean. By combining the four profiles
676 from our study with the CD29-2 profile of Gall et al. (2013), we reconstructed a complete
677 record of Ni isotope variations in seawater over the last ~80 Ma (Figure 8). Besides the light
678 Ni isotope excursion occurring around 48-50 Ma in CD29-2, there is no change in the average
679 oceanic $\delta^{60/58}$Ni value during the last ~80 Ma. This result is important since important oceanic
680 changes (e.g., closing of the Panama gateway, onset of the Northern Hemisphere glaciation)
681 occurred during that period, but didn't produce changes of Ni isotope composition of seawater
682 remains fairly constant during the Cenozoic.
683 The negative Ni isotope excursion observed in CD29-2 Fe-Mn crust (Figure 8) by Gall
684 et al. (2013) and attributed to inputs from hydrothermal sources in the water column, could in
685 fact be the result of Ni isotope fractionation during precipitation and formation processes
686 occurring either in the water column or during formation of the crust, as we have
687 demonstrated for one of our Fe-Mn crusts. The flux of Ni from deep-sea hydrothermal vents
688 is poorly constrained so far (Cameron and Vance, 2014; Little et al., 2015), hence it is unclear
689 how Ni isotope variations in Fe-Mn crusts would respond to hydrothermal input. If lighter Ni
690 isotope compositions are indeed related to hydrothermal inputs, other isotopic proxies and
691 possibly Fe isotopes should also be influenced, which warrant additional studies of other
692 metal isotope systematics in Fe-Mn crusts.
693
694 **5. Conclusions**
695
696 In this study we have reported the geochemical composition and Ni isotope
697 composition of four hydrogenetic Fe-Mn crusts from the North and South Pacific oceans.

Recent Ni isotope compositions reported for hydrogenetic Fe-Mn crusts suggested that Ni isotopes could be used as a tracer of metal sources in modern oceans in particular hydrothermal sources. Here, we demonstrated that Ni isotopes could also be fractionated due to local effects such as alteration processes producing a range of Ni isotope compositions encompassing the total range of $\delta^{60/58}$Ni values measured in Fe-Mn crusts so far. One of the Fe-Mn crusts from the South Pacific presents unusual geochemical variations including high Mn and Ni contents, anomalously high ^{10}Be/^{9}Be ratios, and light $\delta^{60/58}$Ni values in the range of 1.08 to 0.25 ‰ for subsamples close to or in contact with the altered substrate. These results suggest that post-depositional processes involving alteration and reprecipitation processes of Mn-rich oxide phases as well as substrate-seawater interactions have locally affected the geochemical composition of the bottom of the crust. We argue that seawater circulation through fractures within the substrate explains the anomalously high ^{10}Be/^{9}Be ratios in the crust, while rapid reprecipitation of Mn-oxides would have produced large Ni isotope fractionation and preferential incorporation of metals with strong affinity for Mn (e.g., Ni, Cu and Co). We show that despite a light Ni isotope excursion at ~48-50 Ma in one Pacific Fe-Mn crust published in another study, all Ni isotope data obtained so far including our new dataset indicate that the mean $\delta^{60/58}$Ni value in Pacific Fe-Mn crusts has remained constant at ~1.8 ‰ suggesting limited Ni isotope variations of seawater through the Cenozoic. The lack of systematic change in the average $\delta^{60/58}$Ni value of seawater over the last ~80 Ma and the fact that secondary processes involving Ni sorption reactions on Fe-Mn oxides can produce light Ni isotope excursion in Fe-Mn crusts, calls for a critical re-evaluation of the use of Ni isotopes as paleoceanographic proxies. Although we cannot completely rule out the influence of hydrothermal inputs and local sources on the Ni isotope composition of deep seawater and more generally of the effect of variable Ni sources as previously suggested, our results emphasize that enrichment processes and rates of precipitation are likely to be

723 important if not the main factors controlling Ni isotope variations in oceanic Fe-Mn deposits.
724 Our results confirm recent experimental data showing that Ni isotopes fractionate during
725 sorption on Fe- and Mn-oxyhydroxides (Gueguen et al., 2011; Sorensen et al., 2011;
726 Gueguen, 2013; Wasylenki et al., 2014a; Wasylenki et al., 2015). Our results have also
727 implications for interpretation of Ni isotope variations in metalliferous sediments in the deep
728 geological time (e.g., Precambrian Banded Iron Formations) as we showed that precipitated-
729 recrystallization processes may overprint primary Ni isotope systems. The Ni isotope
730 composition of hydrothermal fluids and hydrothermal deposits and whether local Ni sources
731 (e.g., rivers and hydrothermal vents) may be recorded in the Ni isotope composition of Fe-Mn
732 crusts should be also explored in future studies.
733

734 **Acknowledgments:**

735 We thank Philippe Fernagu (Ifremer, Brest, France) for his help during preparation of
736 Fe-Mn crusts samples for microdrilling and Didier Bourlès (CEREGE, Université d'Aix-
737 Marseille, France) for Be isotope analyses. We thank the ROV Jason-II pilots and the crews
738 of the RV Kilo Moana for assistance with deployments and sample collection during the
739 cruise. We also thank the Microbial Observatory Project (FeMO) Principle Investigators:
740 Katrina Edwards (USC), Dave Emerson (Bigelow), Craig Moyer (WWU), Hubert Staudigel
741 (UCSD-SIO), and Brad Tebo (OHSU) for their support and input during cruise operations.
742 Support was provided by the LabexMer ANR-10-LABX-19-01, Europole Mer and FP7
743 (#247837) grant.
744

745 **Figure captions:**
746

747 **Figure 1**: Locations of the sampling sites (A) and photographs of North Pacific Fe-Mn crusts
748 sampling (B and C) using ROV Jason2 during FeMO cruise 2009 on the R/V Kilo Moana
749 (University of Hawaii). Photographs are courtesy of Woods Hole Oceanographic Institution.
750 The map (A) was generated with GeoMapApp (http://www.geomapapp.org/).
751
752 **Figure 2**: Photographs of the four Fe-Mn crusts samples after microdrill sampling using a
753 microdrilling device. Labels "top", "middle", and "bottom" are specified for each Fe-Mn
754 crust. "Top" corresponds to the surface in contact with seawater, "middle" is the part of the
755 crust towards the substrate and "bottom" is when the crust was collected with its substrate,
756 and thus it corresponds to the contact between the crust and substrate. Yellow dashed lines
757 correspond to the positions drilled for making one sample per line drilled. Regions "I" and
758 "O" of crust ZEP2-DR05-04 (D) are noted, and description of these regions are provided in
759 the text.
760
761 **Figure 3**: Ternary diagram plotting Fe, Mn and (Ni+Cu+Co) x 10 concentrations of Fe-Mn
762 crusts from the North Pacific (Apuupuu Seamount) J2-480 and J2-480-R14, and Fe-Mn crusts
763 from the South Pacific (Austral archipelago of French Polynesia) ZEP2-DR05-04 and ZEP2-
764 DR06-03. Lines plotted between points represent the time-series of each Fe-Mn crust. The
765 diagram is adapted from Bonatti et al. (1972) and shows the three fields in which Fe-Mn rich
766 deposits are commonly classified: hydrothermal (light brown area), hydrogenetic (blue area)
767 and diagenetic (yellow area).
768
769 **Figure 4**: Elemental ratios of Fe/Mn, Co/Mn, Ni/Mn and Cu/Mn (g/g) versus depth (mm) in
770 the crust from South Pacific (Austral Archipelago of French Polynesia): ZEP2-DR05-04 and
771 ZEP2-DR06-03 and North Pacific (Apuupuu Seamount). Increasing Ni/Mn in this region "I"

772 in comparison to other part of the crust and to crust ZEP2-DR06-03 indicate that it has
773 undergone geochemical perturbations probably as a result of fluid circulation in the substrate.
774 Increasing Ni/Mn in four data points of crust ZEP2-DR-05-04 are likely not related to
775 variations in growth rates as illustrated by the lack of variations in Fe/Mn (A) and Co/Mn (E)
776 ratios.
777
778 **Figure 5**: Plots of the logarithm of $^{10}Be/^{9}Be$ ratios vs depth in South Pacific (Austral
779 Archipelago of French Polynesia) crusts (A and C) and in North Pacific (Apuupuu Seamount)
780 Fe-Mn crusts (B and D). The red lines in plots A and C show the limit between region "O"
781 (outer) from region "I" (inner) in crust ZEP2-DR05-04 (see text for ample descriptions).
782 Anomalously high $^{10}Be/^{9}Be$ ratios in region "I" of crust ZEP2-DR05-04 (A) likely indicate
783 that seawater fluids circulation in the substrate with high Be isotopes ratios affected the crust
784 directly in contact with the substrate. These fluids promoted alteration of Mn-oxides.
785
786 **Figure 6**: Ni isotope composition (‰) of the Fe-Mn crusts versus depth in the crust. The four
787 Fe-Mn crusts display similar average pattern, with the exception of crust ZEP2-DR05-04
788 showing a decrease in $\delta^{60/58}Ni$ values from an average of ~1.8 ‰ to a value of 0.25 ‰ from
789 ~17 mm to ~22 mm in the crust. The 2sd error shown for our samples on the figure is based
790 on replicate measurements of several geological reference materials (GRMs).
791
792 **Figure 7:** Nickel isotope composition (‰) versus (A) P/Mn, (B) P/Ni, (C) Co/Mn and (D)
793 Mn/Ni ratios (g/g) in the four Fe-Mn crusts. Symbols are for the same as in Figures 4, 5 and 6.
794 The green line in plot (D) represents the linear fitting for the last 5 subsamples of ZEP2-DR-
795 05-04 crust towards the bottom indicating a clear correlation between light Ni isotope
796 compositions and low Mn/Ni ratios, suggesting mixing between two end-members. These

end-members are presumably a hydrogenetic component represented by the average $\delta^{60/58}$Ni value of Fe-Mn crusts from the South Pacific of 1.76 ±0.23 ‰ (2sd) and the $\delta^{60/58}$Ni value of a fluid similar to the substrate (i.e., basalt) in which it has circulated with a value of ~0 ‰.

Figure 8: Time-series of the Ni isotope composition (‰) of South Pacific (Austral Archipelago of French Polynesia) and North Pacific (Apuupuu Seamount) Fe-Mn crusts and the CD29-2 crust profile from Gall et al. (2013). Symbols are identical to those in Figures 4 and 5 for samples from this study and grey triangles represent the CD29-2 crust profile. The blue band represents the range of $\delta^{60/58}$Ni values for modern seawater. Nickel isotope composition is constant and similar within uncertainty in our three Fe-Mn crusts from both North and South Pacific Oceans. The combination of our isotopic profiles from ~0 to ~17 Ma and the CD29-2 profile from ~8 Ma to ~75 Ma implying shows that despite some small Ni isotope excursions the average Ni isotope composition of Pacific deep waters has not varied through Cenozoic and remains at a mean $\delta^{60/58}$Ni value of ~1.8 ‰. The 2sd error shown for our samples on the figure is based on measurements of GRMs replicate.

Table captions:

Table 1: Elemental concentrations (µg/g or wt%) and elemental ratios (g/g), and Ni isotope composition (‰) of North Pacific (Apuupuu) and South Pacific (Tahiti) Fe-Mn crusts.

Table 2: ^{10}Be/^{9}Be ratios, ^{9}Be concentrations (µg/g), Co/Mn ratios (g/g), age (Ma) and growth rates (mm/Ma) of Fe-Mn crusts from North Pacific (Apuupuu) and South Pacific (Tahiti).

References

Abouchami, W., Goldstein, S.L., Galer, S.J.G., Eisenhauer, A. and Mangini, A. (1997) Secular changes of lead and neodymium in central Pacific seawater recorded by a Fe-Mn crust. Geochimica Et Cosmochimica Acta 61, 3957-3974.

Adam, C. and Bonneville, A. (2008) No thinning of the lithosphere beneath northern part of the Cook-Austral volcanic chains. Journal of Geophysical Research: Solid Earth 113, n/a-n/a.

Amend, J.P., McCollom, T.M., Hentscher, M. and Bach, W. (2011) Catabolic and anabolic energy for chemolithoautotrophs in deep-sea hydrothermal systems hosted in different rock types. Geochimica Et Cosmochimica Acta 75, 5736-5748.

Anbar, A.D. and Rouxel, O. (2007) Metal stable isotopes in paleoceanography. Annual Review of Earth and Planetary Sciences 35, 717-746.

Aplin, A.C. and Cronan, D.S. (1985) Ferromanganese oxide deposits from the Central Pacific ocean. 1. Encrustations from the Line islands archipelago. Geochimica Et Cosmochimica Acta 49, 427-436.

Arnold, M., Merchel, S., Bourlès, D.L., Braucher, R., Benedetti, L., Finkel, R.C., Aumaître, G., Gottdang, A. and Klein, M. (2010) The French accelerator mass spectrometry facility ASTER: Improved performance and developments. Nuclear Instruments and Methods in Physics Research Section B: Beam Interactions with Materials and Atoms 268, 1954-1959.

Barling, J., Arnold, G.L. and Anbar, A.D. (2001) Natural mass-dependent variations in the isotopic composition of molybdenum. Earth and Planetary Science Letters 193, 447-457.

Bau, M., Schmidt, K., Koschinsky, A., Hein, J., Kuhn, T. and Usui, A. (2014) Discriminating between different genetic types of marine ferro-manganese crusts and nodules based on rare earth elements and yttrium. Chemical Geology 381, 1-9.

Bonatti, E. and Joensuu, O. (1966) Deep-sea iron deposit from South Pacific. Science 154, 643-&.

Bonatti, E., Kraemer, T. and Rydell, H. (1972) Classification and genesis of submarine iron-manganese deposits, Ferromanganese deposits on the Ocean Floor, D. Horn ed. Washington DC, Nat. Sci. Found., pp. 149-165.

Bonneville, A., Dosso, L. and Hildenbrand, A. (2006) Temporal evolution and geochemical variability of the South Pacific superplume activity. Earth and Planetary Science Letters 244, 251-269.

Bourles, D., Raisbeck, G.M. and Yiou, F. (1989) ^{10}Be and ^{9}Be in marine sediments and their potential for dating. Geochimica Et Cosmochimica Acta 53, 443-452.

Bruland, K.W. (1980) Oceanographic distributions of Cadmium, Zinc, Nickel, and Copper in the North Pacific. Earth and Planetary Science Letters 47, 176-198.

Bruland, K.W. (1983) Trace elements in sea water. Academic Press, London.

Bruland, K.W. and Lohan, M.C. (2003) Controls of Trace Metals in Seawater, in: Heinrich, D.H., Karl, K.T. (Eds.), Treatise on Geochemistry. Pergamon, Oxford, pp. 23-47.

Bruland, K.W., Orians, K.J. and Cowen, J.P. (1994) Reactive trace metals in the stratified central North Pacific. Geochimica Et Cosmochimica Acta 58, 3171-3182.

Bryan, A.L., Dong, S., Wilkes, E.B. and Wasylenki, L.E. (2015) Zinc isotope fractionation during adsorption onto Mn oxyhydroxide at low and high ionic strength. Geochimica et Cosmochimica Acta 157, 182-197.

Cameron, V. and Vance, D. (2014) Heavy nickel isotope compositions in rivers and the oceans. Geochimica Et Cosmochimica Acta 128, 195-211.

Cameron, V., Vance, D., Archer, C. and House, C.H. (2009) A biomarker based on the stable isotopes of nickel. Proceedings of the National Academy of Sciences of the United States of America 106, 10944-10948.

Chen, T.-Y., Ling, H.-F., Hu, R., Frank, M. and Jiang, S.-Y. (2013) Lead isotope provinciality of central North Pacific Deep Water over the Cenozoic. Geochemistry, Geophysics, Geosystems 14, 1523-1537.

Chu, N.C., Johnson, C.M., Beard, B.L., German, C.R., Nesbitt, R.W., Frank, M., Bohn, M., Kubik, P.W., Usui, A. and Graham, I. (2006) Evidence for hydrothermal venting in Fe isotope compositions of the deep Pacific Ocean through time. Earth and Planetary Science Letters 245, 202-217.

Conway, T.M. and John, S.G. (2014) Quantification of dissolved iron sources to the North Atlantic Ocean. Nature 511, 212-215.

Cook, D.L., Clayton, R.N., Wadhwa, M., Janney, P.E. and Davis, A.M. (2008) Nickel isotopic anomalies in troilite from iron meteorites. Geophysical Research Letters 35, L01203.

Craig, J.D., Andrews, J.E. and Meylan, M.A. (1982) Ferromanganese deposits in the hawaiian archipelago. Marine Geology 45, 127-157.

De Carlo, E.H., McMurtry, G.M. and Kim, K.H. (1987) Geochemistry of ferromanganese crusts from the hawaiian archipelago. 1. Northern survey areas. Deep-Sea Research Part a-Oceanographic Research Papers 34, 441-467.

Fitzsimmons, J.N., Boyle, E.A. and Jenkins, W.J. (2014) Distal transport of dissolved hydrothermal iron in the deep South Pacific Ocean. Proceedings of the National Academy of Sciences 111, 16654-16661.

Frank, M. (2002) Radiogenic isotopes: Tracers of past ocean circulation and erosional input. Reviews of Geophysics 40.

Frank, M., O'Nions, R.K., Hein, J.R. and Banakar, V.K. (1999) 60 Myr records of major elements and Pb–Nd isotopes from hydrogenous ferromanganese crusts: reconstruction of seawater paleochemistry. Geochimica Et Cosmochimica Acta 63, 1689-1708.

Frank, M., Whiteley, N., Kasten, S., Hein, J.R. and O'Nions, K. (2002) North Atlantic deep water export to the Southern Ocean over the past 14 Myr: Evidence from Nd and Pb isotopes in ferromanganese crusts. Paleoceanography 17.

Fujii, T., Moynier, F., Dauphas, N. and Abe, M. (2011) Theoretical and experimental investigation of nickel isotopic fractionation in species relevant to modern and ancient oceans. Geochimica et Cosmochimica Acta 75, 469-482.

Gall, L., Williams, H., Siebert, C. and Halliday, A. (2012) Determination of mass-dependent variations in nickel isotope compositions using double spiking and MC-ICPMS. Journal of Analytical Atomic Spectrometry 27, 137-145.

Gall, L., Williams, H.M., Siebert, C., Halliday, A.N., Herrington, R.J. and Hein, J.R. (2013) Nickel isotopic compositions of ferromanganese crusts and the constancy of deep ocean inputs and continental weathering effects over the Cenozoic. Earth and Planetary Science Letters 375, 148-155.

Gueguen, B. (2013) Apport de la géochimie isotopique du Nickel à l'étude des dépôts métallifères océaniques. Thesis, University of Brest.

Gueguen, B., Rouxel, O., Ponzevera, E., Bekker, A. and Fouquet, Y. (2013) Nickel Isotope Variations in Terrestrial Silicate Rocks and Geological Reference Materials Measured by MC-ICP-MS. Geostandards and Geoanalytical Research 37, 297-317.

Gueguen, B., Rouxel, O., Ponzevera, E., Sorensen, J., Toner, B. and Bekker, A. (2011) Ni biogeochemical cycle through geological time: insights from Ni isotope variations in modern and ancient marine metallifereous deposits, AGU Fall Meeting Abstracts, p. 1845.

Halbach, P., Kriete, C., Prause, B. and Puteanus, D. (1989) Mechanisms to explain the platinum concentration in ferromanganese seamount crusts. Chemical Geology 76, 95-106.

Halbach, P. and Puteanus, D. (1984) The influence of the carbonate dissolution rate on the growth and composition of Co-rich ferromanganese crusts from Central Pacific seamount areas. Earth and Planetary Science Letters 68, 73-87.

Halbach, P., Puteanus, D. and Manheim, F.T. (1984) Platinum concentrations in ferromanganese seamount crusts from the Central Pacific. Naturwissenschaften 71, 577-579.

Halbach, P., Segl, M., Puteanus, D. and Mangini, A. (1983) Co-fluxes and growth rates in ferromanganese deposits from Central Pacific seamount areas. Nature 304, 716-719.

Hein, J.R., Bohrson, W.A., Schulz, M.S., Noble, M. and Clague, D.A. (1992) Variations in the fine-scale composition of a Central Pacific ferromanganese crust: paleoceanographic implications. Paleoceanography 7, 63-77.

Hein, J.R., Conrad, T.A., Frank, M., Christl, M. and Sager, W.W. (2012) Copper-nickel-rich, amalgamated ferromanganese crust-nodule deposits from Shatsky Rise, NW Pacific. Geochem. Geophys. Geosyst. 13, Q10022.

Hein, J.R. and Koschinsky, A. (2014) Deep-Ocean Ferromanganese Crusts and Nodules, in: Holland, H.D., Turekian, K.K. (Eds.), Treatise on Geochemistry (Second Edition). Elsevier, Oxford, pp. 273-291.

Hein, J.R., Mizell, K., Koschinsky, A. and Conrad, T.A. (2013) Deep-ocean mineral deposits as a source of critical metals for high- and green-technology applications: Comparison with land-based resources. Ore Geology Reviews 51, 1-14.

Hein, J.R., Schwab, W.C. and Davis, A.S. (1988) Cobalt-rich and platinum-rich ferromanagenese crusts and associated substrate rocks from the Marshall islands. Marine Geology 78, 255-283.

Hein, J.R., Yeh, H.W., Gunn, S.H., Sliter, W.V., Benninger, L.M. and Wang, C.H. (1993) Two major Cenozoic episodes of phosphogenesis recorded in equatorial Pacific seamount deposits. Paleoceanography 8, 293-311.

Henderson, G.M. and Burton, K.W. (1999) Using ($^{234}U/^{238}U$) to assess diffusion rates of isotope tracers in ferromanganese crusts. Earth and Planetary Science Letters 170, 169-179.

Horner, T.J., Schonbachler, M., Rehkämper, M., Nielsen, S.G., Williams, H., Halliday, A.N., Xue, Z. and Hein, J.R. (2010) Ferromanganese crusts as archives of deep water Cd isotope compositions. Geochemistry Geophysics Geosystems 11, 1525-2027.

Horner, T.J., Williams, H.M., Hein, J.R., Saito, M.A., Burton, K.W., Halliday, A.N. and Nielsen, S.G. (2015) Persistence of deeply sourced iron in the Pacific Ocean. Proceedings of the National Academy of Sciences.

Kosakevitch, A. (1987) Platiniferous Fe-Ni cosmic spherules in a marine metalliferous incrustation from Tuamotu (French Polynesia). Comptes Rendus De l'Academie Des Sciences 305, 105-108.

Kosakevitch, A. and Disnar, J.R. (1997) Nature and origin of chemical zoning in the metal nucleus and oxide cortex of cosmic spherules from the Tuamotu Archipelago, French Polynesia. Geochimica Et Cosmochimica Acta 61, 1073-1082.

Koschinsky, A. and Halbach, P. (1995) Sequential leaching of marine ferromanganese precipitates: Genetic implications. Geochimica et Cosmochimica Acta 59, 5113-5132.

Koschinsky, A. and Hein, J.R. (2003) Uptake of elements from seawater by ferromanganese crusts: solid-phase associations and seawater speciation. Marine Geology 198, 331-351.

Koschinsky, A., Stascheit, A., Bau, M. and Halbach, P. (1997) Effects of phosphatization on the geochemical and mineralogical composition of marine ferromanganese crusts. Geochimica et Cosmochimica Acta 61, 4079-4094.

Ku, T.L., Kusakabe, M., Measures, C.I., Southon, J.R., Cusimano, G., Vogel, J.S., Nelson, D.E. and Nakaya, S. (1990) Beryllium isotope distribution in the western North Atlantic: a comparison to the Pacific. Deep-Sea Research Part a-Oceanographic Research Papers 37, 795-808.

Kyte, F.T., Leinen, M., Ross Heath, G. and Zhou, L. (1993) Cenozoic sedimentation history of the central North Pacific: Inferences from the elemental geochemistry of core LL44-GPC3. Geochimica et Cosmochimica Acta 57, 1719-1740.

Lebatard, A.-E., Bourlès, D.L., Duringer, P., Jolivet, M., Braucher, R., Carcaillet, J., Schuster, M., Arnaud, N., Monié, P., Lihoreau, F., Likius, A., Mackaye, H.T., Vignaud, P. and Brunet, M. (2008) Cosmogenic nuclide dating of Sahelanthropus tchadensis and Australopithecus bahrelghazali: Mio-Pliocene hominids from Chad. Proceedings of the National Academy of Sciences 105, 3226-3231.

Lesuave, R., Pichocki, C., Pautot, G., Hoffert, M., Morel, Y., Voisset, M., Monti, S., Amosse, J. and Kosakevitch, A. (1989) Geological and mineralogical study of Co-rich ferromanganese crusts from a submerged atoll in the Tuamotu archipelago (French Polynesia). Marine Geology 87, 227-247.

Levasseur, S., Frank, M., Hein, J.R. and Halliday, A. (2004) The global variation in the iron isotope composition of marine hydrogenetic ferromanganese deposits: implications for seawater chemistry? Earth and Planetary Science Letters 224, 91-105.

Ling, H.-F., Jiang, S.-Y., Frank, M., Zhou, H.-Y., Zhou, F., Lu, Z.-L., Chen, X.-M., Jiang, Y.-H. and Ge, C.-D. (2005) Differing controls over the Cenozoic Pb and Nd isotope evolution of deepwater in the central North Pacific Ocean. Earth and Planetary Science Letters 232, 345-361.

Ling, H.F., Burton, K.W., O'Nions, R.K., Kamber, B.S., von Blanckenburg, F., Gibb, A.J. and Hein, J.R. (1997) Evolution of Nd and Pb isotopes in Central Pacific seawater from ferromanganese crusts. Earth and Planetary Science Letters 146, 1-12.

Little, S.H., Sherman, D.M., Vance, D. and Hein, J.R. (2014b) Molecular controls on Cu and Zn isotopic fractionation in Fe–Mn crusts. Earth and Planetary Science Letters 396, 213-222.

Little, S.H., Vance, D., Lyons, T.W. and McManus, J. (2015) Controls on trace metal authigenic enrichment in reducing sediments: Insights from modern oxygen-deficient settings. American Journal of Science 315, 77-119.

Manheim, F.T. and Lanebostwick, C.M. (1988) Cobalt in ferromanganese crusts as a monitor of hydrothermal discharge on the Pacific seafloor. Nature 335, 59-62.

Morris, J.D. (1991) Applications of cosmogenic ^{10}Be to problems in the Earth sciences. Annual Review of Earth and Planetary Sciences 19, 313-350.

Moynier, F., Blichert-Toft, J., Telouk, P., Luck, J.M. and Albarede, F. (2007) Comparative stable isotope geochemistry of Ni, Cu, Zn, and Fe in chondrites and iron meteorites. Geochimica Et Cosmochimica Acta 71, 4365-4379.

Nicholson, K., Hein, J.R., Buehn, B. and Dasgupta, S. (1997) Manganese mineralization; geochemistry and mineralogy of terrestrial and marine deposits. Geological Society of London : London, United Kingdom.

Nielsen, S.G., Gannoun, A., Marnham, C., Burton, K.W., Halliday, A.N. and Hein, J.R. (2011) New age for ferromanganese crust 109D-C and implications for isotopic records of lead, neodymium, hafnium, and thallium in the Pliocene Indian Ocean. Paleoceanography 26.

Nielsen, S.G., Wasylenki, L.E., Rehkämper, M., Peacock, C.L., Xue, Z. and Moon, E.M. (2013) Towards an understanding of thallium isotope fractionation during adsorption to manganese oxides. Geochimica Et Cosmochimica Acta 117, 252-265.

Nimmo, M., Van Den Berg, C.M.G. and Brown, J. (1989) The chemical speciation of dissolved nickel, copper, vanadium and iron in Liverpool Bay, Irish Sea. Estuarine Coastal and Shelf Science 29, 57-74.

Nishiizumi, K., Kohl, C.P., Arnold, J.R., Klein, J., Fink, D. and Middleton, R. (1991) Cosmic ray produced 10Be and 26Al in Antarctic rocks: exposure and erosion history. Earth and Planetary Science Letters 104, 440-454.

O'Nions, R.K., Frank, M., von Blanckenburg, F. and Ling, H.F. (1998) Secular variation of Nd and Pb isotopes in ferromanganese crusts from the Atlantic, Indian and Pacific Oceans. Earth and Planetary Science Letters 155, 15-28.

Peacock, C.L. (2009) Physiochemical controls on the crystal-chemistry of Ni in birnessite: Genetic implications for ferromanganese precipitates. Geochimica et Cosmochimica Acta 73, 3568-3578.

Peate, D.W., Falkena, L. and Kent, A.J.R. (2009) Pb isotope variations in hydrogenetic Fe-Mn crusts from the Izu-Bonin fore-arc. Chemical Geology 258, 288-298.

Pichocki, C. and Hoffert, M. (1987) Characteristics of Co-rich ferromanganese nodules and crusts sampled in French Polynesia. Marine Geology 77, 109-119.

Puteanus, D. and Halbach, P. (1988) Correlation of Co concentration and growth rate — A method for age determination of ferromanganese crusts. Chemical Geology 69, 73-85.

Ratié, G., Jouvin, D., Garnier, J., Rouxel, O., Miska, S., Guimarães, E., Cruz Vieira, L., Sivry, Y., Zelano, I., Montarges-Pelletier, E., Thil, F. and Quantin, C. (2015) Nickel isotope fractionation during tropical weathering of ultramafic rocks. Chemical Geology 402, 68-76.

Rehkämper, M., Frank, M., Hein, J.R. and Halliday, A. (2004) Cenozoic marine geochemistry of thallium deduced from isotopic studies of ferromanganese crusts and pelagic sediments. Earth and Planetary Science Letters 219, 77-91.

Rehkämper, M., Frank, M., Hein, J.R., Porcelli, D., Halliday, A., Ingri, J. and Liebetrau, V. (2002) Thallium isotope variations in seawater and hydrogenetic, diagenetic, and hydrothermal ferromanganese deposits. Earth and Planetary Science Letters 197, 65-81.

Reynolds, B.C., Frank, M. and O'Nions, R.K. (1999) Nd- and Pb-isotope time series from Atlantic ferromanganese crusts: implications for changes in provenance and paleocirculation over the last 8 Myr. Earth and Planetary Science Letters 173, 381-396.

Rudnick, R.L. and Gao, S. (2014) Composition of the Continental Crust, in: Holland, H.D., Turekian, K.K. (Eds.), Treatise on Geochemistry (Second Edition). Elsevier, Oxford, pp. 1-51.

Schmitt, A.D., Galer, S.J.G. and Abouchami, W. (2009) Mass-dependent cadmium isotopic variations in nature with emphasis on the marine environment. Earth and Planetary Science Letters 277, 262-272.

Sclater, F.R., Boyle, E. and Edmond, J.M. (1976) On the marine geochemistry of nickel. Earth and Planetary Science Letters 31, 119-128.

Segl, M., Mangini, A., Bonani, G., Hofmann, H.J., Nessi, M., Suter, M., Wolfli, W., Friedrich, G., Pluger, W.L., Wiechowski, A. and Beer, J. (1984) ^{10}Be-dating of a manganese crust from Central North Pacific and implications for ocean palaeocirculation. Nature 309, 540-543.

Siebert, C., Nagler, T.F. and Kramers, J.D. (2001) Determination of molybdenum isotope fractionation by double-spike multicollector inductively coupled plasma mass spectrometry. Geochemistry Geophysics Geosystems 2, 1032.

Siebert, C., Nagler, T.F., von Blanckenburg, F. and Kramers, J.D. (2003) Molybdenum isotope records as a potential new proxy for paleoceanography. Earth and Planetary Science Letters 211, 159-171.

Sorensen, J.V., Toner, B.M., Gueguen, B. and Rouxel, O. (2011) Ni Speciation and Isotope Fractionation in Marine Ferromangenese Deposits. Goldschmidt Conference 2011 75, 1914.

Staudigel, H. and Hart, S.R. (1983) Alteration of basaltic glass: Mechanisms and significance for the oceanic crust-seawater budget. Geochimica Et Cosmochimica Acta 47, 337-350.

Staudigel, H., Plank, A., White, B. and Schminke, H., -U., (1996) Geochemical fluxes during seafloor alteration of the basaltic upper oceanic crust : DSDP sites 417 and 418. Geophysical Monograph Series vol. 96, 19-38.

Steinhilber, F., Abreu, J.A., Beer, J., Brunner, I., Christl, M., Fischer, H., Heikkilä, U., Kubik, P.W., Mann, M., McCracken, K.G., Miller, H., Miyahara, H., Oerter, H. and Wilhelms, F. (2012) 9,400 years of cosmic radiation and solar activity from ice cores and tree rings. Proceedings of the National Academy of Sciences 109, 5967-5971.

Stuart, F.M. and Lee, M.R. (2012) Micrometeorites and extraterrestrial He in a ferromanganese crust from the Pacific Ocean. Chemical Geology 322–323, 209-214.

Tagliabue, A., Bopp, L., Dutay, J.C., Bowie, A.R., Chever, F., Jean-Baptiste, P., Bucciarelli, E., Lannuzel, D., Remenyi, T., Sarthou, G., Aumont, O., Gehlen, M. and Jeandel, C. (2010) Hydrothermal contribution to the oceanic dissolved iron inventory. Nature Geoscience 3, 252-256.

Tanaka, S. and Inoue, T. (1979) ^{10}Be of North Pacific sediment cores up to 2.5 million years BP. Earth and Planetary Science Letters 45, 181-187.

Toner, B.M., Fakra, S.C., Manganini, S.J., Santelli, C.M., Marcus, M.A., Moffett, J., Rouxel, O., German, C.R. and Edwards, K.J. (2009) Preservation of iron(II) by carbon-rich matrices in a hydrothermal plume. Nature Geoscience 2, 197-201.

Turner, A., Nimmo, M. and Thuresson, K.A. (1998) Speciation and sorptive behaviour of nickel in an organic-rich estuary (Beaulieu, UK). Marine Chemistry 63, 105-118.

van de Flierdt, T., Frank, M., Halliday, A.N., Hein, J.R., Hattendorf, B., Günther, D. and Kubik, P.W. (2003) Lead isotopes in North Pacific deep water - implications for past changes in input sources and circulation patterns. Earth and Planetary Science Letters 209, 149-164.

van de Flierdt, T., Frank, M., Halliday, A.N., Hein, J.R., Hattendorf, B., Günther, D. and Kubik, P.W. (2004) Tracing the history of submarine hydrothermal inputs and the significance of hydrothermal hafnium for the seawater budget—a combined Pb–Hf–Nd isotope approach. Earth and Planetary Science Letters 222, 259-273.

Van Den Berg, C.M.G. and Nimmo, M. (1987) Determination of interactions of Nickel with dissolved organic material in seawater using cathodic stripping voltammetry. Science of the Total Environment 60, 185-195.

von Blanckenburg, F., O'Nions, R.K., Belshaw, N.S., Gibb, A. and Hein, J.R. (1996a) Global distribution of beryllium isotopes in deep ocean water as derived from Fe-Mn crusts. Earth and Planetary Science Letters 141, 213-226.

von Blanckenburg, F., O'Nions, R.K. and Hein, J.R. (1996b) Distribution and sources of pre-anthropogenic lead isotopes in deep ocean water from Fe-Mn crusts. Geochimica Et Cosmochimica Acta 60, 4957-4963.

Wasylenki, L., Wells, R. and Spivak-Birndorf, L. (2014a) Ni Sorption to Birnessite Drives a Surprisingly Large Fractionation, AGU Fall Meeting Abstracts, p. 3623.

Wasylenki, L.E., Howe, H.D., Spivak-Birndorf, L.J. and Bish, D.L. (2015) Ni isotope fractionation during sorption to ferrihydrite: Implications for Ni in banded iron formations. Chemical Geology 400, 56-64.

Wasylenki, L.E., Rolfe, B.A., Weeks, C.L., Spiro, T.G. and Anbar, A.D. (2008) Experimental investigation of the effects of temperature and ionic strength on Mo isotope fractionation during adsorption to manganese oxides. Geochimica Et Cosmochimica Acta 72, 5997-6005.

Wasylenki, L.E., Swihart, J.W. and Romaniello, S.J. (2014b) Cadmium isotope fractionation during adsorption to Mn oxyhydroxide at low and high ionic strength. Geochimica et Cosmochimica Acta 140, 212-226.

Wasylenki, L.E., Weeks, C.L., Bargar, J.R., Spiro, T.G., Hein, J.R. and Anbar, A.D. (2011) The molecular mechanism of Mo isotope fractionation during adsorption to birnessite. Geochimica Et Cosmochimica Acta 75, 5019-5031.

Willenbring, J.K. and von Blanckenburg, F. (2010a) Long-term stability of global erosion rates and weathering during late-Cenozoic cooling. Nature 465, 211-214.

Willenbring, J.K. and von Blanckenburg, F. (2010b) Meteoric cosmogenic Beryllium-10 adsorbed to river sediment and soil: Applications for Earth-surface dynamics. Earth-Science Reviews 98, 105-122.

Zhu, X.K., O'Nions, R.K., Guo, Y.L. and Reynolds, B.C. (2000) Secular variation of iron isotopes in North Atlantic Deep Water. Science 287, 2000-2002.

Table 1: Elemental concentrations, elemental ratios, and Ni isotope composition of North Pacific (Apuupuu) and South Pacific (Tahiti) Fe-Mn crusts.

Sample name	Depth in the crust (mm)	Mn (wt%)	Fe (wt%)	Al (µg/g)	Ti (µg/g)	Ca (µg/g)	P (µg/g)	Co (µg/g)	Ni (µg/g)	Cu (µg/g)	Zn (µg/g)	Fe/Mn	Ni/Mn	Cu/Mn	Zn/Mn	Ni/Co	Ti/Al	Al/Fe	P/Ni	$\delta^{60/58}$Ni (‰)	2se (‰)
ZEP2-DR05-04 Fe-Mn crust																					
Average		**10.31**	**8.36**	**3996**	**7693**	**14466**	**3646**	**5462**	**2002**	**548**	**345**									**1.72**	**0.17 (2sd)**
ZEP2-DR05-04-L1	0.5	17.07	8.95	3604	11864	17876	3662	12406	2790	383	395	0.52	0.016	0.0022	0.0023	0.22	3.29	0.04	1.31	1.89	0.04
ZEP2-DR05-04-L2	1	13.53	8.12	2809	9051	14012	2386	8922	2483	410	335	0.60	0.018	0.0030	0.0025	0.28	3.22	0.03	0.96	1.82	0.05
ZEP2-DR05-04-L3	2.5	15.71	8.77	3998	10937	15973	3230	8495	2919	564	417	0.56	0.019	0.0036	0.0027	0.34	2.74	0.05	1.11	1.69	0.03
ZEP2-DR05-04-L4	3.5	11.02	7.23	3351	8808	12023	2334	5536	2063	435	327	0.66	0.019	0.0040	0.0030	0.37	2.63	0.05	1.13	1.71	0.03
ZEP2-DR05-04-L5	4.5	7.37	6.59	2868	6520	8593	1944	3047	1287	328	229	0.89	0.017	0.0044	0.0031	0.42	2.27	0.04	1.51	1.65	0.02
ZEP2-DR05-04-L6	6.5	8.33	7.96	3697	7181	10927	2838	3750	1259	422	261	0.95	0.015	0.0051	0.0031	0.34	1.94	0.05	2.25	1.75	0.04
ZEP2-DR05-04-L7	8.5	12.76	11.90	4883	9760	19372	5969	5882	1919	674	414	0.93	0.015	0.0053	0.0032	0.33	2.00	0.04	3.11	1.74	0.03
ZEP2-DR05-04-L8	10	9.84	9.50	3917	7785	13743	4033	4782	1464	576	341	0.97	0.015	0.0059	0.0035	0.31	1.99	0.04	2.75	1.81	0.03
ZEP2-DR05-04-L9	11.5	9.32	8.62	3478	7014	17582	5784	4684	1365	545	316	0.93	0.015	0.0058	0.0034	0.29	2.02	0.04	4.24	1.72	0.03
ZEP2-DR05-04-L10	12.5	9.91	9.62	3208	6555	11675	2950	5483	1459	533	314	0.97	0.015	0.0054	0.0032	0.27	2.04	0.03	2.02	1.67	0.04
ZEP2-DR05-04-L11	13.5	8.19	8.30	2885	5669	10238	2574	4226	1240	476	260	1.01	0.015	0.0058	0.0032	0.29	1.97	0.03	2.08	1.63	0.03
ZEP2-DR05-04-L12	15.5	7.60	7.44	3558	5760	11681	2844	3952	1336	515	276	0.98	0.018	0.0068	0.0036	0.34	1.62	0.05	2.13	1.54	0.03
ZEP2-DR05-04-L13	16.5	7.33	7.69	3140	5436	11421	3131	3675	1188	465	248	1.05	0.016	0.0063	0.0034	0.32	1.73	0.04	2.64	1.69	0.02
ZEP2-DR05-04-L14	17.5	12.98	11.37	6809	9821	21638	6105	6346	2753	947	529	0.88	0.021	0.0073	0.0041	0.43	1.44	0.06	2.22	1.08	0.03
ZEP2-DR05-04-L15	19	7.48	6.95	3966	5251	14892	3748	3150	1871	555	337	0.93	0.025	0.0074	0.0045	0.59	1.32	0.06	2.00	1.01	0.04
ZEP2-DR05-04-L16	20	10.13	7.99	6070	8280	17988	4239	5205	3238	810	473	0.79	0.032	0.0080	0.0047	0.62	1.36	0.08	1.31	0.63	0.04
ZEP2-DR05-04-L17	22	6.64	5.07	5694	5089	16289	4215	3321	3395	670	403	0.76	0.051	0.0101	0.0061	1.02	0.89	0.11	1.24	0.25	0.05

Table 1: continued

Sample name	Depth in the crust (mm)	Mn (wt%)	Fe (wt%)	Al (µg/g)	Ti (µg/g)	Ca (µg/g)	P (µg/g)	Co (µg/g)	Ni (µg/g)	Cu (µg/g)	Zn (µg/g)	Fe/Mn	Ni/Mn	Cu/Mn	Zn/Mn	Ni/Co	Ti/Al	Al/Fe	P/Ni	$\delta^{60/58}$Ni (‰)	2se (‰)
ZEP2-DR06-03 Fe-Mn crust																					
Average		**8.78**	**8.23**	**3601**	**7586**	**44011**	**7707**	**4843**	**1248**	**473**	**257**									**1.87**	**0.10 (2sd)**
ZEP2-DR06-03-L1	0.5	11.41	7.87	2079	8037	12804	2923	8694	1682	293	255	0.69	0.015	0.0026	0.0022	0.19	3.87	0.03	1.74	1.88	0.04
ZEP2-DR06-03-L2	2.5	12.38	9.77	3484	10527	14623	3687	7774	1745	451	304	0.79	0.014	0.0036	0.0025	0.22	3.02	0.04	2.11	1.94	0.02
ZEP2-DR06-03-L3	4	12.46	9.96	3660	11517	14250	3575	7225	1777	483	317	0.80	0.014	0.0039	0.0025	0.25	3.15	0.04	2.01	1.86	0.04
ZEP2-DR06-03-L4	5.5	9.53	8.33	2764	8890	10726	2871	5385	1320	393	254	0.87	0.014	0.0041	0.0027	0.25	3.22	0.03	2.17	1.89	0.04
ZEP2-DR06-03-L5	7.5	7.72	10.09	3621	10999	11741	3278	3948	1011	420	328	1.31	0.013	0.0054	0.0042	0.26	3.04	0.04	3.24	1.84	0.03
ZEP2-DR06-03-L6	9.5	9.69	8.30	3794	7393	21139	3010	4907	1687	477	259	0.86	0.017	0.0049	0.0027	0.34	1.95	0.05	1.78	1.95	0.03
ZEP2-DR06-03-L7	11	8.56	7.78	4380	7062	21185	3347	3552	1279	480	239	0.91	0.015	0.0056	0.0028	0.36	1.61	0.06	2.62	1.89	0.03
ZEP2-DR06-03-L8	12.5	8.38	8.20	4312	7047	27977	3886	3952	1134	504	245	0.98	0.014	0.0060	0.0029	0.29	1.63	0.05	3.43	1.89	0.03
ZEP2-DR06-03-L9	14	8.36	8.52	4277	6783	48600	4067	4299	1146	557	258	1.02	0.014	0.0067	0.0031	0.27	1.59	0.05	3.55	1.87	0.03
ZEP2-DR06-03-L10	16	6.93	7.41	3743	5682	74906	5642	3551	972	492	230	1.07	0.014	0.0071	0.0033	0.27	1.52	0.05	5.81	1.80	0.03
ZEP2-DR06-03-L11	17.5	7.49	8.14	3948	6102	73244	8949	3954	1015	562	247	1.09	0.014	0.0075	0.0033	0.26	1.55	0.05	8.81	1.84	0.04
ZEP2-DR06-03-L12	19	6.96	7.03	3289	5546	71144	11887	3570	916	500	222	1.01	0.013	0.0072	0.0032	0.26	1.69	0.05	12.97	1.87	0.04
ZEP2-DR06-03-L13	21	6.82	7.46	3723	5554	95379	19236	3729	912	516	226	1.09	0.013	0.0076	0.0033	0.24	1.49	0.05	21.10	1.86	0.03
ZEP2-DR06-03-L14	23.5	6.27	6.40	3335	5062	118434	31536	3255	881	490	211	1.02	0.014	0.0078	0.0034	0.27	1.52	0.05	35.78	1.75	0.03

Table 1: continued

Sample name	Depth in the crust (mm)	Mn (wt%)	Fe (wt%)	Al (µg/g)	Ti (µg/g)	Ca (µg/g)	P (µg/g)	Co (µg/g)	Ni (µg/g)	Cu (µg/g)	Zn (µg/g)	Fe/Mn	Ni/Mn	Cu/Mn	Zn/Mn	Ni/Co	Ti/Al	Al/Fe	P/Ni	$\delta^{60/58}$Ni (‰)	2se (‰)
J2-480 Fe-Mn crust																					
Average		**14.06**	**9.89**	**4097**	**7781**	**54630**	**24651**	**3045**	**2122**	**1124**	**574**									**1.65**	**0.19 (2sd)**
J2-480-R1	0.2	10.95	9.30	2794	10066	67980	32497	2749	730	663	582	0.85	0.007	0.0061	0.0053	0.48	3.60	0.03	44.51	1.72	0.07
J2-480-R2	2.5	11.23	7.80	1665	8039	47308	21279	2540	1629	843	465	0.69	0.014	0.0075	0.0041	0.94	4.83	0.02	13.07	1.74	0.03
J2-480-R3	5	9.91	7.10	1471	6220	31367	13294	2294	1355	795	458	0.72	0.014	0.0080	0.0046	0.97	4.23	0.02	9.81	1.65	0.07
J2-480-R4	7	14.87	9.59	2132	8925	45545	19196	4341	2118	1204	614	0.65	0.014	0.0081	0.0041	0.92	4.19	0.02	9.06	1.66	0.03
J2-480-R5	9	22.81	10.27	2176	8790	35156	11551	5574	3597	1837	761	0.45	0.016	0.0081	0.0033	0.95	4.04	0.02	3.21	1.67	0.04
J2-480-R6	11	19.83	11.55	2485	9252	69904	31549	4507	2814	1411	692	0.58	0.014	0.0071	0.0035	0.90	3.72	0.02	11.21	1.65	0.07
J2-480-R7	12.5	18.32	10.81	2829	9900	84690	39523	3709	2863	1331	709	0.59	0.016	0.0073	0.0039	0.90	3.50	0.03	13.81	1.72	0.05
J2-480-R8	14	17.21	9.84	2845	7906	61954	28104	2953	3001	1300	659	0.57	0.017	0.0076	0.0038	0.93	2.78	0.03	9.36	1.65	0.03
J2-480-R9	15	15.30	11.96	4224	7231	66488	30368	2809	2817	1310	644	0.78	0.018	0.0086	0.0042	0.94	1.71	0.04	10.78	-	-
J2-480-R10	16.5	8.01	11.54	9245	4765	59716	29250	1095	1225	888	432	1.44	0.015	0.0111	0.0054	0.95	0.52	0.08	23.88	1.64	0.04
J2-480-R12	19	6.16	9.03	13204	4499	30826	14550	917	1190	779	293	1.46	0.019	0.0126	0.0048	0.99	0.34	0.15	12.23	1.41	0.03

Table 1:continued

Sample name	Depth in the crust (mm)	Mn (wt%)	Fe (wt%)	Al (µg/g)	Ti (µg/g)	Ca (µg/g)	P (µg/g)	Co (µg/g)	Ni (µg/g)	Cu (µg/g)	Zn (µg/g)	Fe/Mn	Ni/Mn	Cu/Mn	Zn/Mn	Ni/Co	Ti/Al	Al/Fe	P/Ni	$\delta^{60/58}$Ni (‰)	2se (‰)
J2-480-R14 Fe-Mn crust																					
Average		**15.18**	**10.41**	**4341**	**7988**	**13325**	**2404**	**4749**	**3209**	**949**	**698**									**1.79**	**0.13 (2sd)**
J2-480-R14-L11	0.2	15.56	11.82	4952	9779	13237	2750	4691	3048	712	850	0.76	0.020	0.0046	0.0055	0.65	1.97	0.04	0.90	1.94	0.03
J2-480-R14-L10	3	12.95	10.73	5972	9719	11778	2376	3720	2554	707	945	0.83	0.020	0.0055	0.0073	0.69	1.63	0.06	0.93	1.81	0.03
J2-480-R14-L9	5	14.66	10.87	5936	10458	13635	2579	4707	3036	841	924	0.74	0.021	0.0057	0.0063	0.64	1.76	0.05	0.85	1.75	0.03
J2-480-R14-L8	7	17.31	10.36	6500	9819	13693	2661	5414	3325	911	630	0.60	0.019	0.0053	0.0036	0.61	1.51	0.06	0.80	1.78	0.04
J2-480-R14-L7	9	16.03	9.37	3441	9087	13503	2126	5977	3443	948	576	0.58	0.021	0.0059	0.0036	0.58	2.64	0.04	0.62	1.86	0.03
J2-480-R14-L6	10	17.38	9.71	2180	8542	14658	2378	6250	3819	1037	735	0.56	0.022	0.0060	0.0042	0.61	3.92	0.02	0.62	1.80	0.05
J2-480-R14-L5	12	13.74	10.53	2917	8317	13802	2330	5267	3156	1008	593	0.77	0.023	0.0073	0.0043	0.60	2.85	0.03	0.74	1.74	0.05
J2-480-R14-L4	14	16.40	10.00	2458	6755	14323	2118	5613	3447	1061	758	0.61	0.021	0.0065	0.0046	0.61	2.75	0.02	0.61	1.78	0.03
J2-480-R14-L3	16	18.51	11.76	3468	5845	14249	2523	4384	3680	1193	650	0.64	0.020	0.0064	0.0035	0.84	1.69	0.03	0.69	1.81	0.04
J2-480-R14-L2	18	13.18	10.44	4445	5020	12142	2261	3401	3048	1075	552	0.79	0.023	0.0082	0.0042	0.90	1.13	0.04	0.74	1.74	0.03
J2-480-R14-L1	20	11.23	8.96	5480	4522	11554	2340	2811	2737	950	471	0.80	0.024	0.0085	0.0042	0.97	0.83	0.06	0.85	1.70	0.03
Nod-P-1	-	-	-	-		-		-	-	-	-	-	-	-	-	-	-			0.34	0.04 (2sd)**
Nod-A-1	-	-	-	-		-		-	-	-	-	-	-	-	-	-	-			1.06	0.04 (2sd)

**2sd was caluclate on replicate measurements (see text for details).

Table 2: $^{10}Be/^{9}Be$ ratios, ^{9}Be concentrations, Co/Mn ratios, age and growth rates of Fe-Mn crusts from North Pacific (Apuupuu) and South Pacific (Tahiti).

Sample name	Depth in the crust (mm)	Co/Mn	^{9}Be (µg/g)	$^{10}Be/^{9}Be$	Age* (Ma)	Growth rate** (mm/Ma)	Age (Ma)
ZEP2-DR05-04 Fe-Mn crust							
ZEP2-DR05-04-L1	0.5	0.073	2.6	1.02E-08	-	-	-
ZEP2-DR05-04-L2	1	0.066	2.0	na	-	-	-
ZEP2-DR05-04-L3	2.5	0.054	2.6	na	-	-	-
ZEP2-DR05-04-L4	3.5	0.050	2.5	na	-	-	-
ZEP2-DR05-04-L5	4.5	0.041	1.9	na	-	-	-
ZEP2-DR05-04-L6	6.5	0.045	2.9	7.41E-09	-	-	-
ZEP2-DR05-04-L7	8.5	0.046	4.1	na	-	-	-
ZEP2-DR05-04-L8	10	0.049	3.4	na	-	-	-
ZEP2-DR05-04-L9	11.5	0.050	3.2	na	-	-	-
ZEP2-DR05-04-L10	12.5	0.055	2.9	6.50E-09	-	-	-
ZEP2-DR05-04-L11	13.5	0.052	2.6	na	-	-	-
ZEP2-DR05-04-L12	15.5	0.052	2.5	na	-	-	-
ZEP2-DR05-04-L13	16.5	0.050	2.2	na	-	-	-
ZEP2-DR05-04-L14	17.5	0.049	4.0	1.40E-07	-	-	-
ZEP2-DR05-04-L15	19	0.042	2.2	na	-	-	-
ZEP2-DR05-04-L16	20	0.051	2.7	na	-	-	-
ZEP2-DR05-04-L17	22	0.050	1.4	4.31E-08	-	-	-
ZEP2-DR06-03 Fe-Mn crust							
ZEP2-DR06-03-L1	0.5	0.076	2.0	6.91E-08	0.9	-	0.9
ZEP2-DR06-03-L2	2.5	0.063	3.0	na	-	-	2.1
ZEP2-DR06-03-L3	4	0.058	3.0	na	-	-	3.1
ZEP2-DR06-03-L4	5.5	0.057	2.6	na	-	-	4.0
ZEP2-DR06-03-L5	7.5	0.051	3.1	8.35E-09	5.2	1.45	5.2
ZEP2-DR06-03-L6	9.5	0.051	2.3	na			5.5
ZEP2-DR06-03-L7	11	0.042	2.3	6.07E-09	5.8	1.89	5.8
ZEP2-DR06-03-L8	12.5	0.047	2.6	na	-	-	5.9
ZEP2-DR06-03-L9	14	0.051	2.4	na	-	-	6.0
ZEP2-DR06-03-L10	16	0.051	2.2	na	-	-	6.0
ZEP2-DR06-03-L11	17.5	0.053	2.4	5.20E-09	6.1	2.86	6.1
ZEP2-DR06-03-L12	19	0.051	2.1	na			6.3
ZEP2-DR06-03-L13	21	0.055	2.2	4.28E-09	6.5	3.23	6.5
ZEP2-DR06-03-L14	23.5	0.052	2.2	3.51E-09	6.9	3.40	6.9
J2-480 Fe-Mn crust							
J2-480-R1	0.2	0.025	6.1	3.14E-09	7.1	-	7.1
J2-480-R2	2.5	0.023	4.6	na	-	-	7.4
J2-480-R3	5	0.023	4.3	na	-	-	7.7
J2-480-R4	7	0.029	5.3	na	-	-	7.9
J2-480-R5	9	0.024	4.8	na	-	-	8.2
J2-480-R6	11	0.023	5.7	na	-	-	8.4
J2-480-R7	12.5	0.020	6.1	na	-	-	8.6
J2-480-R8	14	0.017	5.3	1.40E-09	8.7	1.60	8.7
J2-480-R9	15	0.018	6.2	na	-	-	9.4
J2-480-R10	16.5	0.014	6.1	na	-	-	10.4
J2-480-R12	19	0.015	4.7	2.71E-10	12.0	1.58	12.0
J2-480-R14 Fe-Mn crust							
J2-480-R14-L11	0.2	0.030	3.6	1.75E-08	3.7	-	3.7
J2-480-R14-L10	3	0.029	3.7	na	-	-	5.5
J2-480-R14-L9	5	0.032	4.0	3.81E-09	6.7	0.74	6.7
J2-480-R14-L8	7	0.031	3.9	na	-	-	7.8
J2-480-R14-L7	9	0.037	3.5	1.32E-09	8.9	1.01	8.9
J2-480-R14-L6	10	0.036	3.6	na	-	-	9.4
J2-480-R14-L5	12	0.038	5.0	na	-	-	10.5
J2-480-R14-L4	14	0.034	4.0	3.53E-10	11.5	1.22	11.5
J2-480-R14-L3	16	0.024	4.5	na	-	-	12.4
J2-480-R14-L2	18	0.026	3.9	1.50E-10	13.2	1.36	13.2
J2-480-R14-L1	20	0.025	3.9	2.31E-11	17.0	1.18	17.0

*Derived from Be isotopes.

**[illegible]

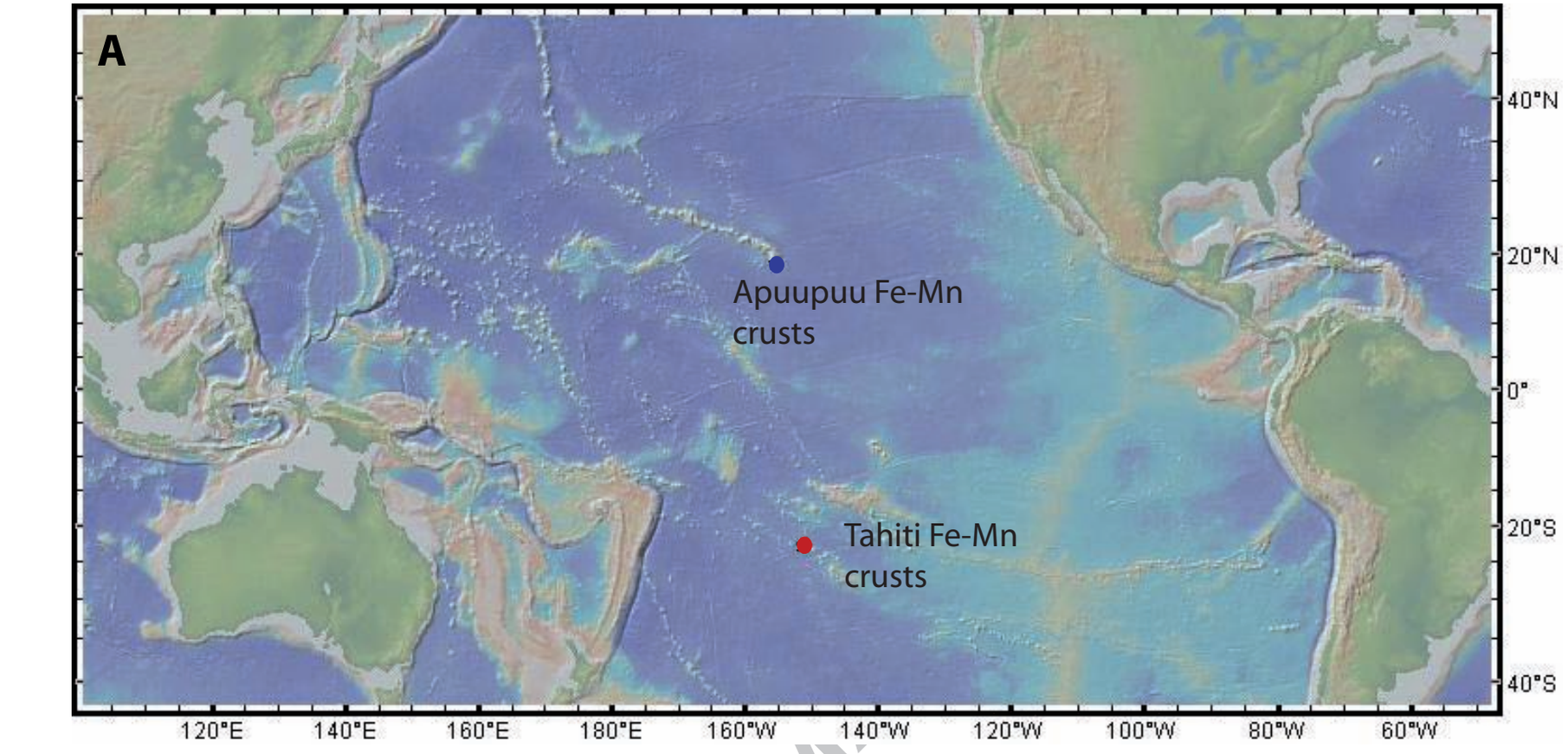

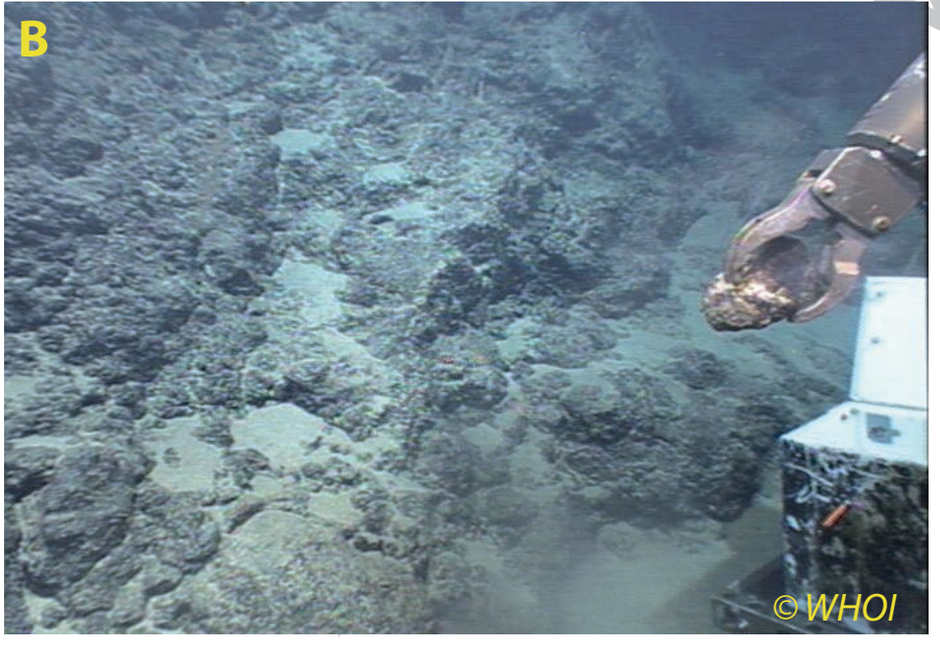

Figure 1

Figure 2

(A)

J2-480-R14

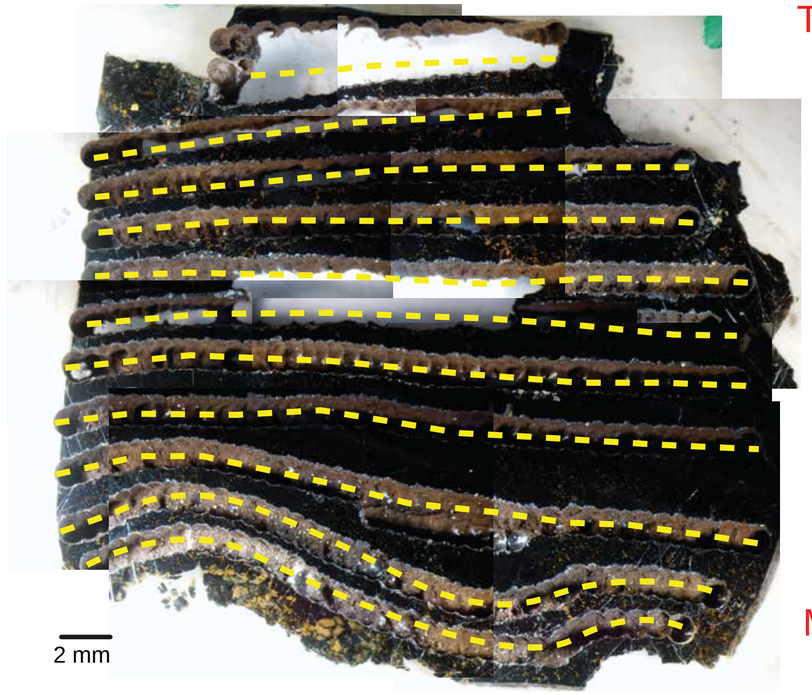

(B)

J2-480

(C)

ZEP2-DR06-03

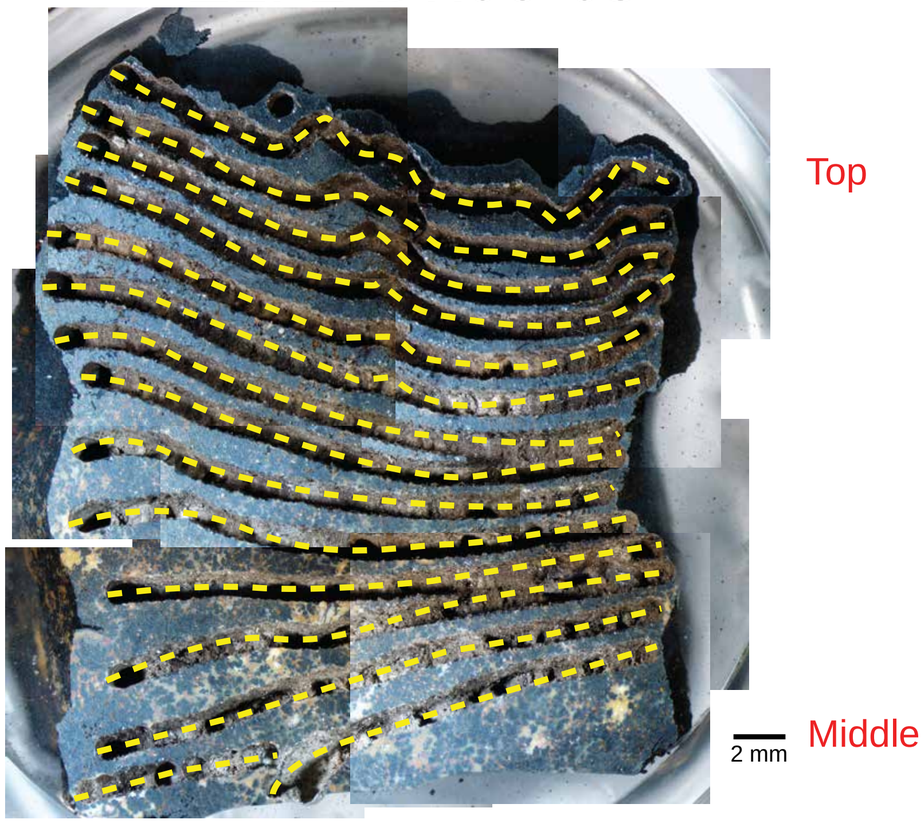

(D)

ZEP2-DR05-04

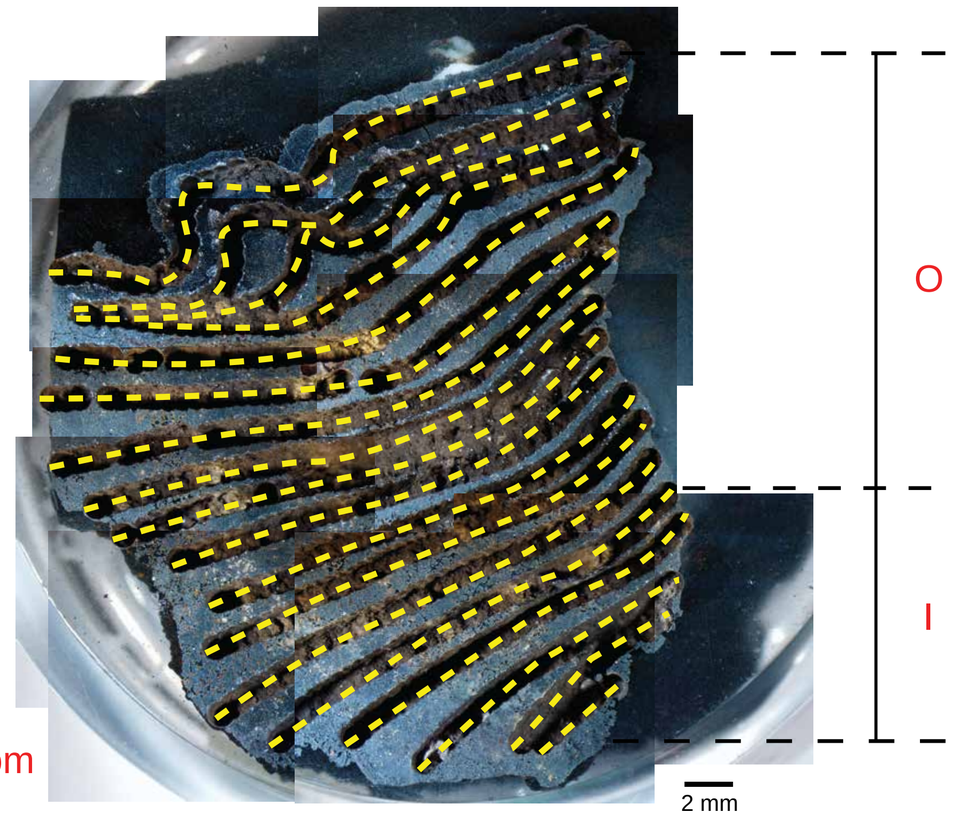

Figure

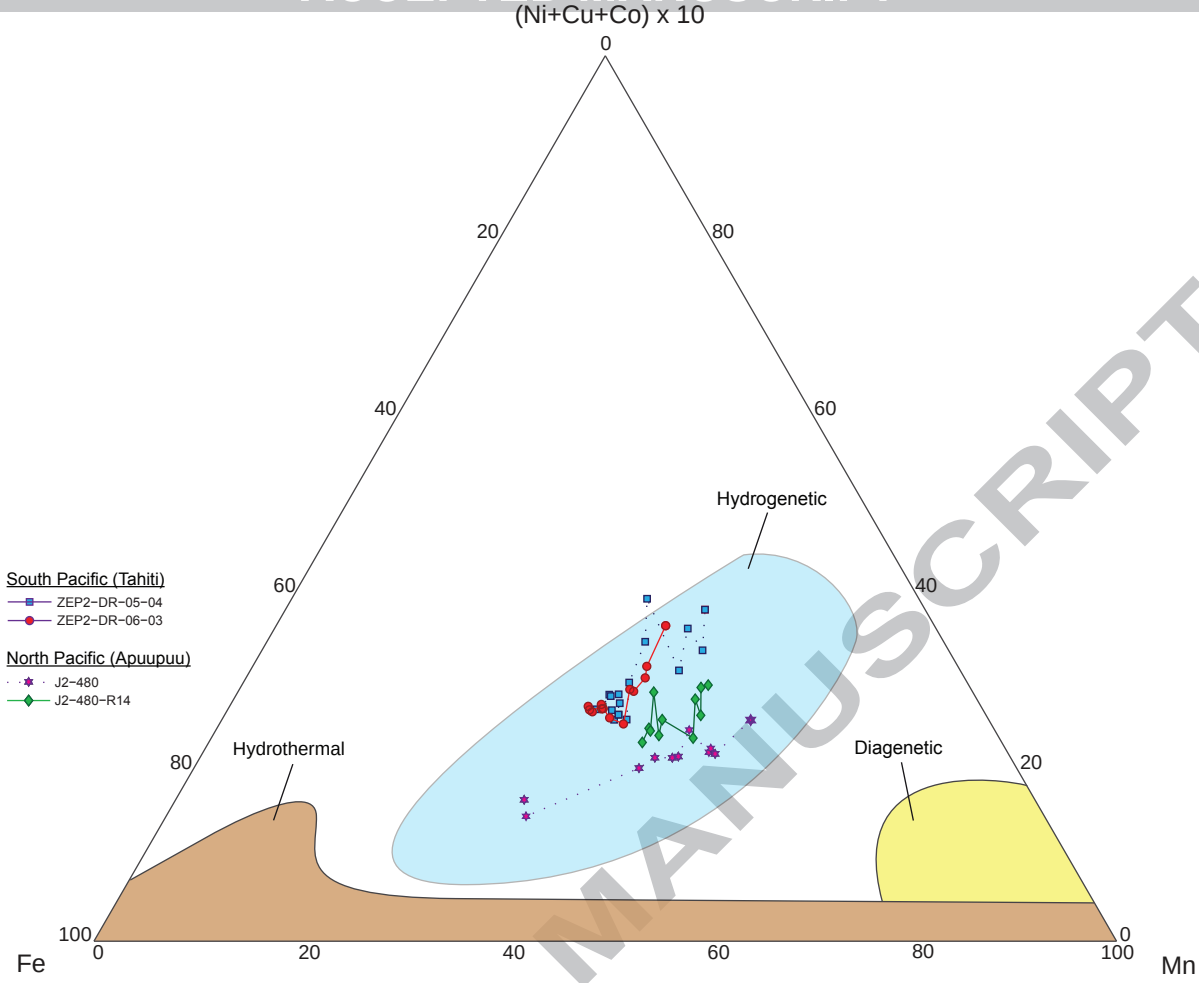

Figure 3

Figure

South Pacific

North Pacific

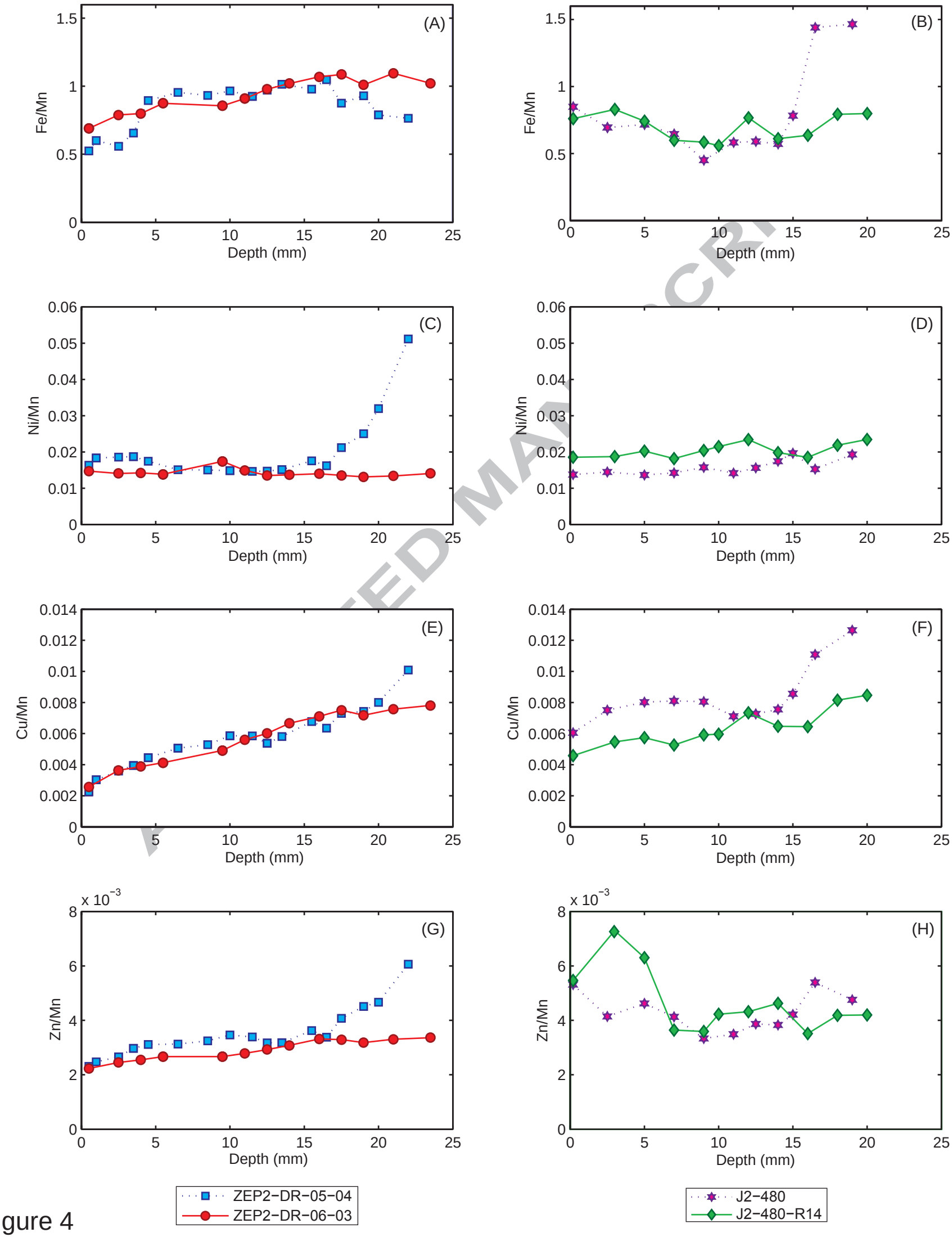

Figure 4

Figure

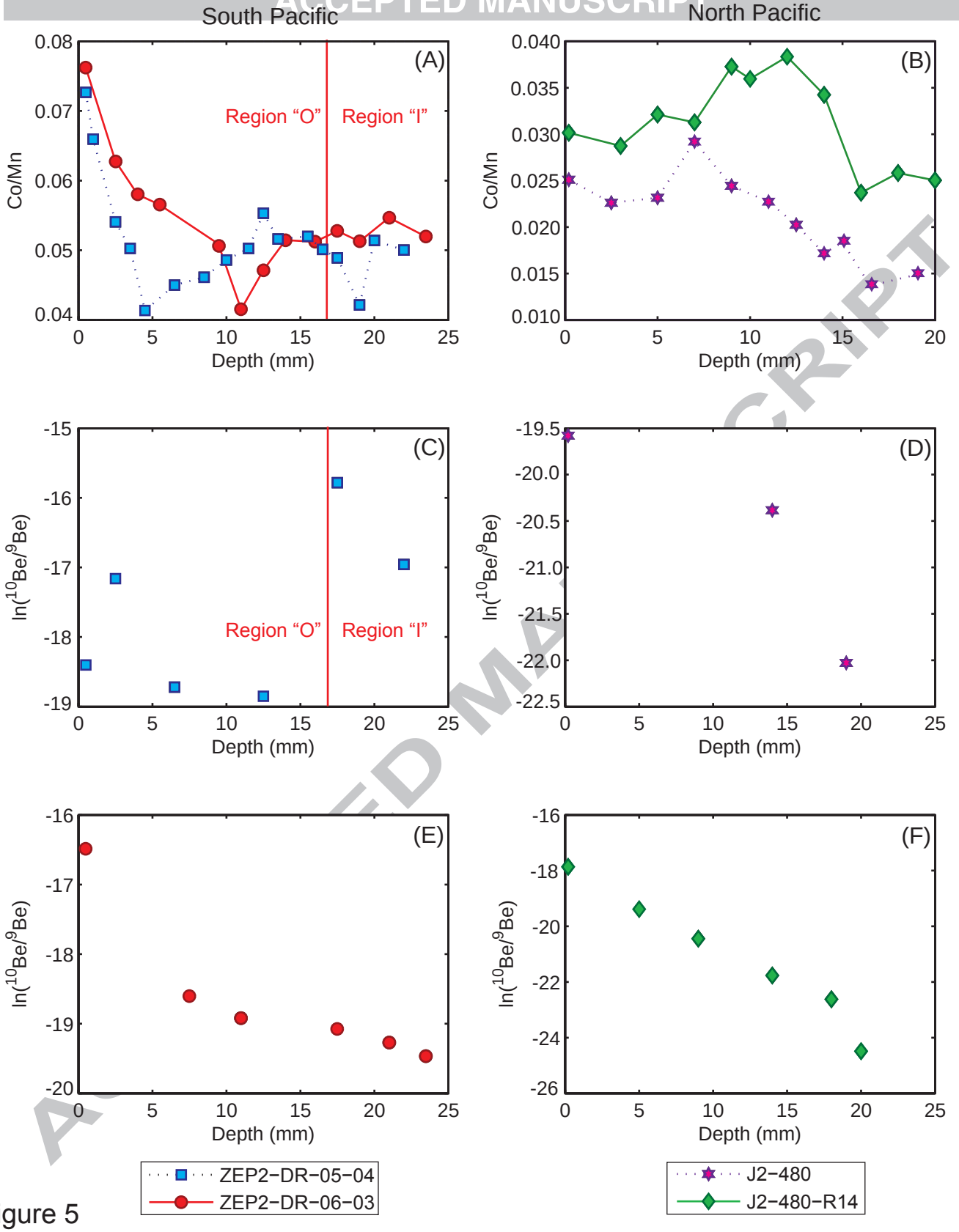

Figure 5

Figure

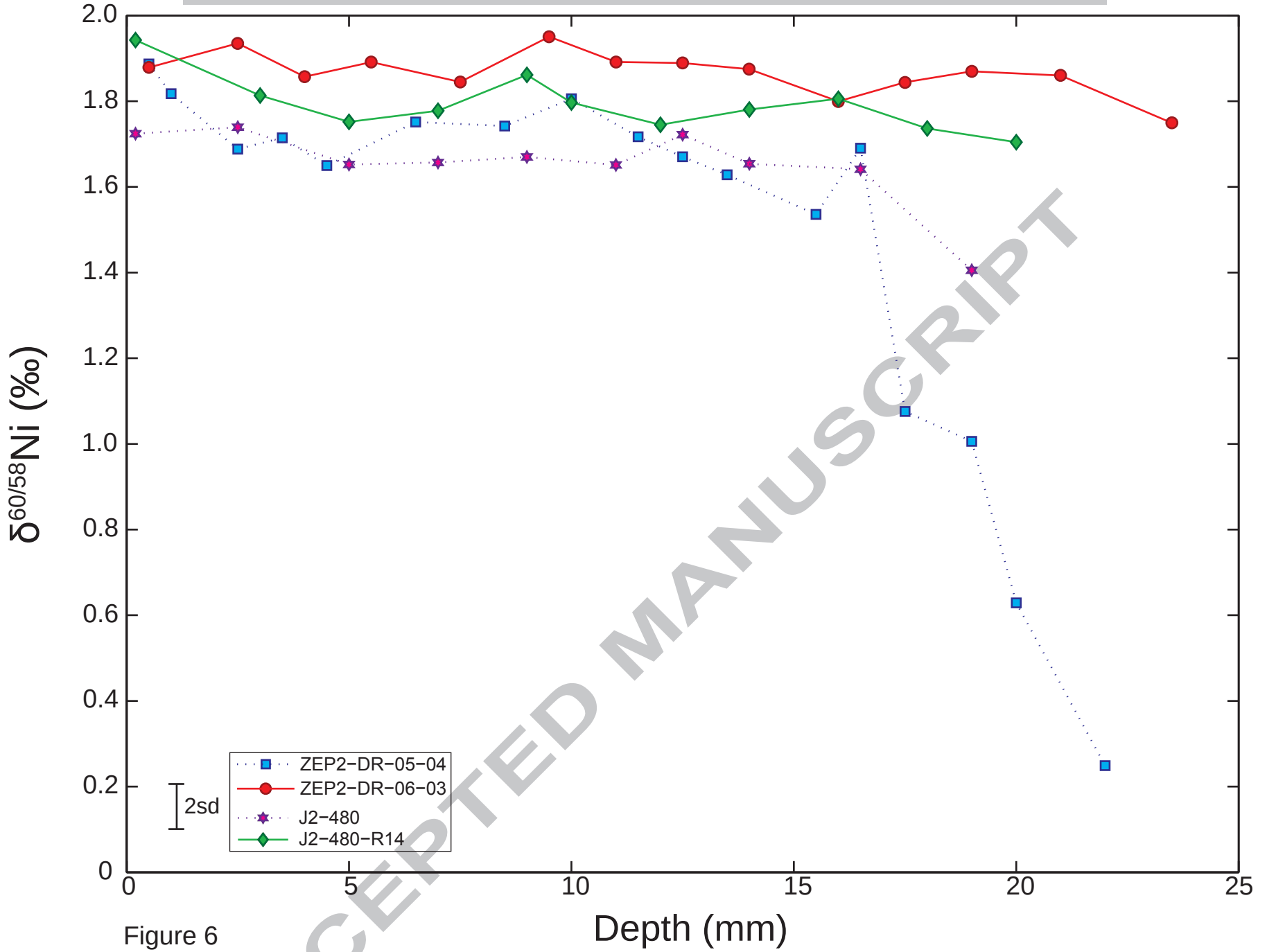

Figure 6

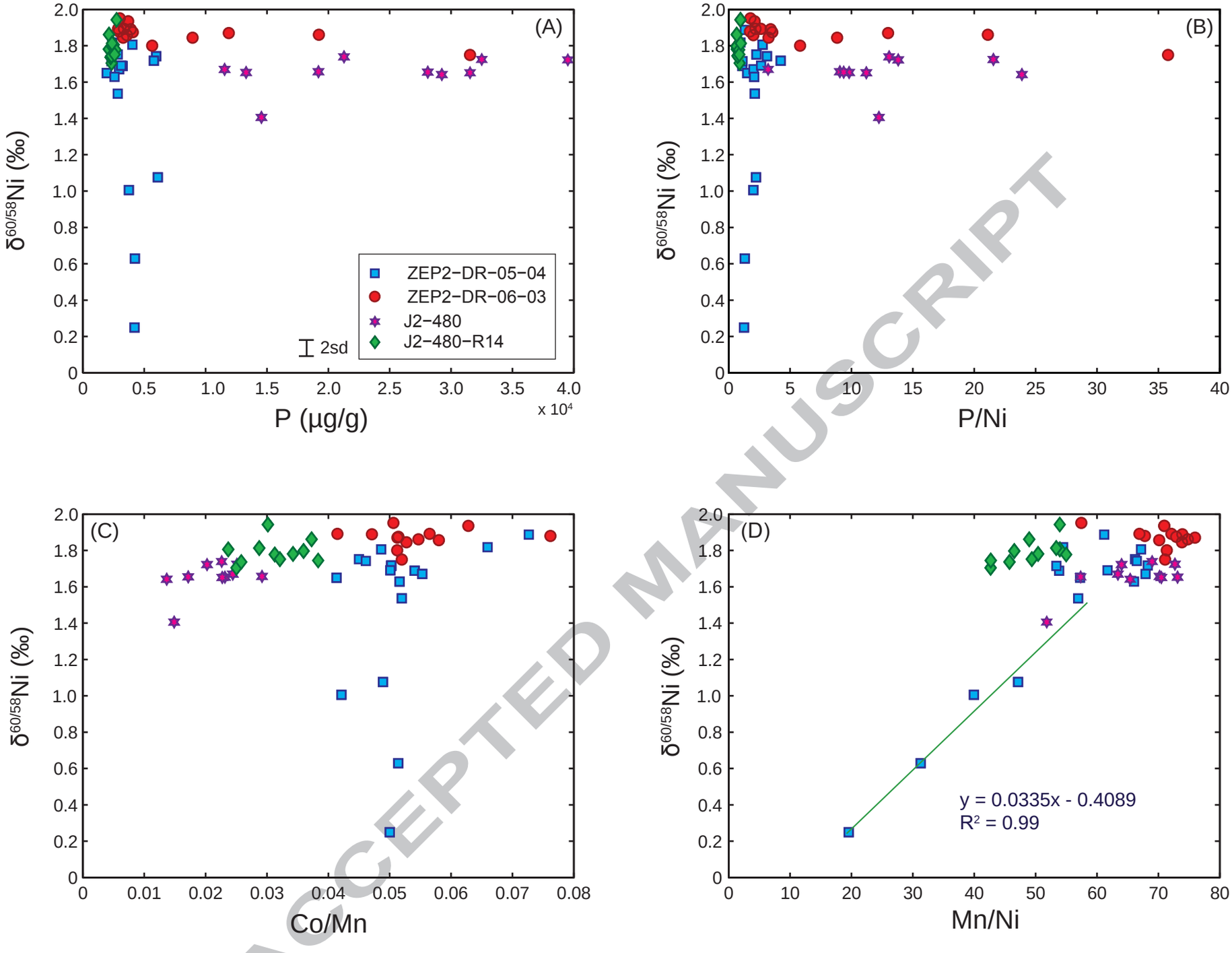

Figure 7

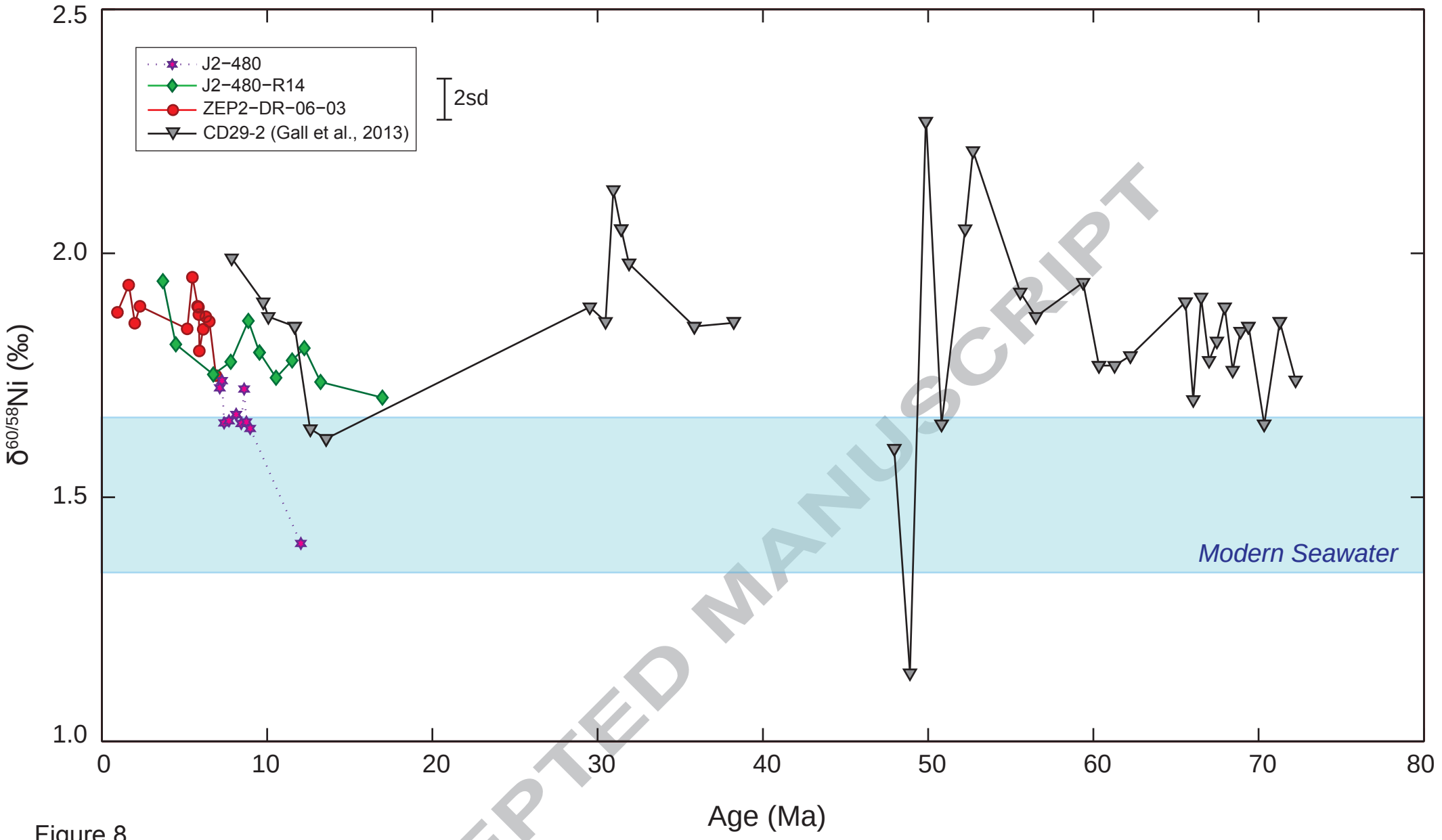

Figure 8